JVI Accepted Manuscript Posted Online 15 January 2020
J. Virol. doi:10.1128/JVI.01024-19
Copyright © 2020 American Society for Microbiology. All Rights Reserved.

Accepted Manuscript Posted Online
Journal of Virology
JVI
Journal of Virology

Downloaded from http://jvi.asm.org/ on February 4, 2020 at 26989832

Capsid labelled HIV to investigate the role of capsid during nuclear import and integration

Irena Zurnic Bönisch[a], Lieve Dirix[a,b] , Veerle Lemmens[b,c], Doortje Borrenberghs[b], Flore De Wit[a], Frank Vernaillen[d,e], Susana Rocha[b], Frauke Christ[a], Jelle Hendrix[c], Johan Hofkens[b] , Zeger Debyser[a,*]

Author affiliations

[a] Laboratory for Molecular Virology and Gene Therapy, Department of Pharmaceutical and Pharmacological Sciences, KU Leuven, Herestraat 49, 3000 Leuven, Flanders, Belgium; [b] Laboratory for Photochemistry and Spectroscopy, Molecular Imaging and Photonics, Department of Chemistry, KU Leuven, Celestijnenlaan 200F, 3001 Heverlee, Flanders, Belgium; [c] Dynamic Bioimaging Lab, Advanced Optical Microscopy Centre and Biomedical Research Institute, Hasselt University, B-3590 Diepenbeek, Belgium; [d] VIB Bioinformatics Core, Rijvisschestraat 126 3R, 9052 Zwijnaarde, Belgium; [e] VIB Bioimaging Core, Herestraat 49, Box 602, 3000 Leuven, Belgium

Author contact information:
Irena Zurnic Bönisch: irena_bios@yahoo.com.sg
Lieve Dirix: lieve.dirix@gmail.com
Veerle Lemmens: veerle.lemmens@uhasselt.be
Doortje Borrenberghs: doortjeborrenberghs@gmail.com
Flore De Wit: flore.dewit@kuleuven.be
Frank Vernaillen: Frank.Vernaillen@vib.be
Susana Rocha : susana.rocha@kuleuven.be
Frauke Christ : frauke.christ@kuleuven.be
Jelle Hendrix : jelle.hendrix@uhasselt.be
Johan Hofkens : johan.hofkens@kuleuven.be

[*] Corresponding author: zeger.debyser@kuleuven.be

Abstract word count: 199; Text word count: 10076

Accepted Manuscript Posted Online

Abstract

The HIV-1 capsid protein performs multiple roles in virus replication both during assembly and particle release and during virus trafficking into the nucleus. In order to decipher the roles of capsid protein during early replication, a reliable method to follow its intracellular distribution is required. To complement existing approaches to track HIV-1 capsid during early infection, we developed an HIV-1 imaging strategy, relying on viruses incorporating eGFP-tagged capsid (CA-eGFP) protein and mCherry-tagged integrase (IN-mCherry). Wild type infectivity and sensitivity to inhibition by PF74 point to the functionality of CA-eGFP containing complexes. Low numbers of CA-eGFP molecules are located inside the viral core and imported in the nucleus without significant loss in intensity. Less than 5% of particles carrying both CA-eGFP and IN-mCherry retain both labelled proteins after nuclear entry implying a major uncoating event at the nuclear envelope dissociating IN and CA. Still, 20% of all CA-eGFP containing complexes are detected in the nucleus. Unlike for IN-mCherry complexes, addition of the integrase inhibitor raltegravir had no effect on CA-eGFP containing complexes, suggesting that these may be not (yet) competent for integration. Our imaging strategy offers alternative visualization of viral capsid trafficking and helps clarify its potential role during integration.

Importance

HIV-1 capsid protein (CA) builds a conical shell protecting viral genomic RNA inside the virus particles. Upon entry into host cells, this shell disassembles in a process of uncoating, which is coordinated with reverse transcription of viral RNA into DNA. After uncoating, a portion of CA remains associated with the viral DNA, mediates its nuclear import and, potentially, integration into host DNA. In this study, we tagged CA with eGFP to follow its trafficking in host cells and address potential CA roles in the nucleus. We found that, while functional viruses import the tagged CA into the nucleus, this capsid protein is not part of integration competent complexes. The roles of nuclear CA thus remain to be established.

Journal of Virology

JVI

Journal of Virology

Downloaded from http://jvi.asm.org/ on February 4, 2020 at 26989832

Accepted Manuscript Posted Online

Keywords: HIV, capsid, fluorescence imaging, CA-eGFP, integration, nuclear import

Background

The HIV-1 capsid protein (CA) is a 24 kDa-large structural protein, which builds a conical shell inside the viral envelope (reviewed in 1). The capsid shell shields the viral RNA genome, the enzymes associated with it and viral accessory proteins. The central role of the capsid protein (CA) during early HIV-1 replication steps has been well established (reviewed in 1). During its fusion with the host cell, HIV-1 releases a capsid core into the cytosol. The conical HIV-1 core is composed of approximately 1500 CA monomers (2, 3, 4) and has a dual role. On the one hand, it is stable enough to protect viral DNA in the pre-integration complexes (PICs) from degradation in the cytoplasm (5, 6, 7, 8) and simultaneously it is flexible enough to allow timely uncoating coordinated with reverse transcription (9). It remains under debate how and when this uncoating occurs, either by opening of pores or a cap on the short end of the capsid core (10) or by entire core disintegration (11). Two models of the timing of uncoating prevail: cytosolic uncoating versus uncoating at the nuclear pore. Evidence for cytosolic uncoating comes from observations with HIV carrying Gag-internal GFP (Gag-iGFP) polyprotein (12, 13); iGFP is present in viral cores and released into the cytosol within the first 30 min post fusion (11). Further support stems from findings that the sensitivity of HIV-1 to TRIM-Cyp is progressively lost during the first 4 h post infection (14, 15, 16). In contrast with this model, other data suggest that uncoating occurs after docking to the nuclear pore. In fact, intact HIV-1 cores were observed at the nuclear envelope (NE) by electron microscopy (EM) (17) and viral DNA was found to remain protected from cytosolic degradation for a prolonged time after infection (7, 8). Recently, live-cell imaging experiments of cells transduced with CypA-dsRed labelled HIV-1 particles demonstrated that only viruses that retain the CypA-dsRed capsid core marker until docking to the

Journal of Virology
JVI
Journal of Virology
Downloaded from http://jvi.asm.org/ on February 4, 2020 at 26989832

Accepted Manuscript Posted Online

Journal of Virology

JVI

Journal of Virology

Downloaded from http://jvi.asm.org/ on February 4, 2020 at 26989832

83 nuclear envelope are infectious (18). The latter data thus support the view that the capsid core is
84 structurally retained until reaching the NE and only undergoes uncoating at this point.
85 Reverse transcription results in the formation of the viral PIC, which contains HIV DNA and integrase
86 (IN) along with other viral and cellular proteins. Although to date no evidence exists for a direct
87 effect of CA on integrase activity (19), recent data propose a role for CA during nuclear import of HIV-
88 1 PICs (20, 21, 22). Whether this role is restricted to docking of PICs on the cytoplasmic side of the
89 nucleopore (e.g. through NUP358), involves capsid uncoating when stalled in the nuclear basket (e.g.
90 through NUP153) or is mediated by a direct interaction between capsid and nuclear import factors is
91 not known. Despite contradictory models on the exact location of uncoating, there is a growing
92 consensus that small amounts of CA protein can be detected in the host cell nucleus during early
93 infection (23, 24, 25). The amount of nuclear CA is lower than what is present in intact incoming
94 cores and its role is not understood. Nuclear CA reportedly co-localizes with either vDNA and/or the
95 viral protein R (Vpr) (23, 24, 25), but there is no consensus on whether this is a hallmark of
96 integration-competent viral complexes. Furthermore, it remains to be shown if CA traverses the
97 nuclear envelope in association with the PIC or by an alternative, PIC-independent route. Given the
98 interaction of CA with nucleoporins Nup 153 and Nup358 (22, 55), it is possible for CA oligomers to
99 enter the nucleus on their own and aid the active nuclear import of PIC. Furthermore, interaction
100 between HIV-1 CA and cleavage and polyadenylation specificity factor 6 (CPSF6) has been implied to
101 mediate CA nuclear import and targeting of CA-decorated PICs to favorable chromatin regions in the
102 host cell nucleus (22, 50, 51, 56, 57).
103 The pleiotropic role of capsid during HIV-1 replication has stimulated research on inhibitors targeting
104 CA function/uncoating, with PF74 being one of the most investigated compounds (26, 27). PF74
105 binds the interhexameric interface on the capsid core lattice, perturbs capsid stability and blocks PIC
106 nuclear import (22, 23, 27, 28, 29). At high concentrations (≥ 10 μM), PF74 also blocks reverse
107 transcription (23, 29, 30). PF74 can thus be used as a research tool to investigate mechanisms by
108 which CA contributes to the formation, trafficking and possibly integration of HIV-1 PICs.

Accepted Manuscript Posted Online

Journal of Virology

JVI

Journal of Virology

Downloaded from http://jvi.asm.org/ on February 4, 2020 at 26989832

Traditionally, CA is labelled in infected cells by immunostaining, with results and interpretations depending on the protocol used (11, 18, 23-25). For this reason, demonstrating the presence of CA in the nucleus was challenging until recently and a consensus protocol on how to best stain for nuclear CA is lacking. Direct p24 tagging through tetracysteine motif (tC) insertions has been described before (37-38), but this labelling still requires a secondary step of FlAsH dye attachment to the tC motif, which is technically demanding. In this study, we explored a method to enable direct imaging of the CA protein distribution in the host cells, by generating particles containing CA C-terminally tagged with enhanced green fluorescent protein (eGFP). By combining CA-eGFP labelling with mCherry-labelling of viral integrase (IN-mCherry), we can simultaneously track the fate of both viral proteins during early infection. We used the capsid inhibitor PF74 and the integrase strand transfer inhibitor raltegravir (RAL) to study the functionality of the CA-eGFP containing complexes in the cytoplasm and the nucleus. We believe our data provide relevant insights into distribution of the fluorescently labelled HIV-1 CA, making it a useful tool to study early HIV-1 replication steps.

Results

A new and direct HIV-1 capsid labelling strategy

To attempt and simplify CA tagging inside infected cells, we developed a direct capsid labelling strategy through fusion of CA with enhanced green fluorescent protein (eGFP). We started by comparing insertions or terminal attachments of tC tags with terminal attachments of eGFP to CA (Figure 1A and C). We used two different tC tags: the short CCPGCC (for insertions within the CA sequence; Figure 1A and 1B) and the longer, modified tag FLNCCPGCCMEP (52) (for N- and C-terminal tagging of the CA; Figure 1C), which has an increased affinity for FlAsH and increases signal quantum yield. As outlined in Material and Methods, we used two different linkers for tagging of CA with eGFP, based on the described linker properties (31) and to facilitate minimal interference with CA structure (Figure 1C). To attach eGFP to the N-terminus of CA we used a flexible glycine-serine linker (GGSGT) and for the C-terminal fusion we used a proline-kink (DPPVAT) linker. We next assessed the

Accepted Manuscript Posted Online

Journal of Virology

JVI

Journal of Virology

Downloaded from http://jvi.asm.org/ on February 4, 2020 at 26989832

tC and eGFP N- and C-terminal fusions to CA for their ability to support efficient virus production (Figure 1D). We produced replication-deficient viruses containing only the tagged CA versions and those with different ratios of tagged to untagged CA. The ratios refer to the amounts of coding plasmids used for transfection. Virus particles were concentrated, and particle release was measured by p24 ELISA and SG-PERT (see Material and Methods). All labelling approaches resulted in reduced particle release and infectivity (Figure 1D), in line with the described fragility of the CA for proper cone formation (2). Additionally, we measured the single-round transduction efficiency of all tagged viruses, using a luciferase reporter in HeLa P4 cells (Figure 2). Lowering the ratio of CA-eGFP to untagged CA in the particles to 1:10 rescued transduction capacity of all dually-tagged particles. In contrast, the 1:2 ratio of CA-eGFP versus untagged CA only yielded luciferase signals with eGFP-tagged CA and the N-terminally positioned tC tag in CA (N-terminal tC and tC_{4-9}). Viruses produced with only the tagged CA versions (ratio 1:0 in the figure legend) were unable to transduce target cells (Figure 2). In further experiments, we tested if these labelled particles can be visualized by fluorescence microscopy through either FlAsH labelling (for tC modified CA; data not shown) or by eGFP fluorescence (data not shown). Since it was not possible to perform successful FlAsH labelling despite extensive optimization according to published protocols (11, 37), we decided to continue with the CA construct C-terminally tagged with eGFP (CA-eGFP).

To develop an integrated particle visualization approach, the CA labelling strategy was applied to a previously established and characterized virus labelling system containing the fluorescently tagged IN (32, 33). Briefly, in this system, the IN protein with a C-terminal fluorescent tag (IN-FP) is packaged into virions by Vpr-mediated transincorporation. After proteolytic cleavage from Vpr, the IN-FP fusion becomes a functional component of the viral PIC. As a modification of this approach and to make IN labelling compatible with CA-eGFP, we used the mCherry tagged IN in the same vector (IN-mCherry). We first validated the use of IN-mCherry in our system, by comparing particle release and transduction efficiency of IN-mCherry containing particles with the previously published IN-eGFP labelled viruses (Figure 3) (33, 34). Both the p24 ELISA and quantitative RT tests showed comparable

Accepted Manuscript Posted Online

Journal of Virology

JVI

Journal of Virology

Downloaded from http://jvi.asm.org/ on February 4, 2020 at 26989832

161 virus production efficiencies (Figure 3A). Subsequently, normalized amounts of each virus (according
162 to either p24 ELISA or SG-PERT qPCR) were used to transduce HeLa P4 cells and single-round
163 infectivity was assayed by luciferase reporter (fLuc) readout three days post transduction (Figure 3B).
164 Both the IN-mCherry and IN-eGFP labelled viruses efficiently transduced target cells, demonstrating
165 the functionality of these viruses. To ensure that the IN-FP incorporation and labelling efficiency
166 were comparable between these two virus species, we spotted purified and concentrated viruses on
167 coverslips and immunostained them with the p24 antibody (Figure 3C). We observed that the
168 fluorescence background was higher in the IN-mCherry channel (Figure 3C, upper panel) which
169 impaired reliable determination of particle labelling efficiency, in contrast to IN-eGFP containing
170 viruses (Figure 3C, lower panel). Since the high mCherry background could also originate from
171 background fluorescence of extracellular vesicles or the coverslip surface, we decided to validate
172 these viruses in virus imaging experiments. Transduced HeLa P4 cells were fixed 6 h post infection
173 and IN-FP localization and content were probed by the IN-FP intracellular distribution (Figure 3D),
174 efficiency of nuclear entry (Figure 3E) and IN-FP fluorescence intensity profiles (Figure 3F) as
175 described previously (33) (Figure 3 D-F). Since all data were comparable between the two viral
176 species, without background interference in the IN-mCherry channel, we conclude that IN-mCherry is
177 a suitable particle label. Hence, we continued with further characterization of double-labelled viruses
178 containing IN-mCherry and CA-eGFP.
179 To produce capsid labelled virus particles, we used a mixture of pNL4.3.Luc.R-E- based plasmids
180 coding for tagged and untagged CA at different ratios: 1:0, 1:2, 1:10 or 0:1, respectively (CA-eGFP
181 coding vector versus untagged, original pNL4.3.Luc.R-E- vector). This pNL4.3.Luc.R-E- mixture was
182 transiently cotransfected with Vpr-IN-mCherry and VSV-G encoding constructs into 293T cells to
183 produce double labelled HIV-1 particles (Figure 4A). As a reference, unlabelled particles (termed WT)
184 and single labelled particles (termed wild type-mCherry, WT-mCh) were produced by transfection of
185 the original pNL4.3.Luc.R-E- in combination with only the VSV-G encoding or both the VSV-G and IN-
186 mCherry encoding constructs, respectively. Vpr transincorporation of fluorescently tagged Vpr-IN is

Accepted Manuscript Posted Online

Journal of Virology

JVI

Journal of Virology

Downloaded from http://jvi.asm.org/ on February 4, 2020 at 26989832

187 known not to influence single-round virus infectivity (32, 33), as confirmed in this study (compare
188 WT and WT-mCh conditions in Figure 4C). Virus production efficiency was determined by the
189 endogenous RT qPCR test. We confirm that fusing eGFP tag to p24 CA diminishes virus particle
190 release, which can be restored to varying levels by producing particles with a mixture of untagged
191 and tagged CA (Figure 1D and 4B). Estimating the functionality of these particles for single round
192 transduction, we observed that increasing the ratio of untagged to eGFP-tagged CA in the virions
193 rescued single round transduction efficiency (Figure 4C). Hence, it is possible to introduce the eGFP
194 label to the HIV-1 capsid without detrimental effects on particle release and virus transduction
195 efficiency.
196 Next, we addressed the CA-eGFP labelling efficiency and the extent of dual particle labelling (Figure
197 5). To this end, we spotted the single- or double labelled particles in 8-well microscopy chambers,
198 fixed and stained them with the capsid-specific monoclonal antibody to determine the percentage of
199 particles (all foci stained with p24 antibody) containing CA-eGFP (Figure 5A). Based on previous data
200 reporting high particle labelling efficiency for IN-eGFP (34), we expect IN-mCherry to be present in a
201 comparable fraction of all particles. As previously shown (Figure 3C), the relatively high fluorescence
202 background in the mCherry channel hampered an exact estimation of IN-mCherry labelling efficiency
203 in the virus particles. When looking at the CA-eGFP positive foci, about 30% of particles (as detected
204 by p24 immunostaining) contained the capsid label (Figure 5B).
205 Based on the one to ten CA-eGFP to parental pNL4-3.luc construct ratio during virus production, we
206 expect that one tenth of all CA molecules in the virion should be labelled with eGFP. This
207 theoretically amounts to about 400 CA-eGFP molecules out of a total of 4000 CA monomers (4).
208 Thus, we next determined how many CA-eGFP monomers were part of the mature virions. To this
209 end, we subjected purified and concentrated CA-eGFP labelled virions to single particle intensity
210 analysis using wide-field total internal reflection fluorescence (TIRF) microscopy (Figure 5C), as
211 described previously (34). In brief, we coated coverslips with CA-eGFP virus solutions at
212 concentrations at which single viruses could be discriminated and compared the intensity

Accepted Manuscript Posted Online

Journal of Virology

JVI

Journal of Virology

Downloaded from http://jvi.asm.org/ on February 4, 2020 at 26989832

213 determined by 2D Gaussian fitting of these viruses with the intensity of coated single eGFP
214 molecules. From the single virus intensity, we determined that between one and four eGFP
215 molecules (indicative of the same number of CA-eGFP monomers with a median number of two) are
216 found in the labelled viruses. Thus, the CA-eGFP labelling efficiency of the recombinant HIV-1 virions
217 is low, which may result from the sterical hindrance the eGFP tag exerts on the capsid core.
218 To confirm that the eGFP signal in imaged viruses originated from the CA-eGFP fusion and not free
219 eGFP, we lysed concentrated virus particles and virus-producing 293T cells and subjected these
220 lysates to Western blotting (Figure 5D). We produced viruses containing either only IN-mCherry (WT-
221 mCh lanes) or both IN-mCherry and CA-eGFP (CA-eGFP lanes). In these experiments, we produced
222 CA-eGFP tagged viruses by co-transfecting three different ratios of the CA-eGFP luciferase transfer
223 vector to the parental vector (1:2, 1:5 and 1:10, as indicated in the blot). We detected Gag and capsid
224 protein variants in these samples using both the p24- and GFP-specific antibodies. Non-transfected
225 cell lysates (labelled mock, m) were used as a negative control. We detected both the Gag precursor
226 protein with additional eGFP (pr55 Gag-eGFP) and CA-eGFP in virus producing cells transfected with
227 the pNL4-3.Luc.R-E- based vector mixtures. When analyzing virus particle lysates, we observed a
228 dominant CA-eGFP band, as well as minor bands corresponding to the Gag precursor (Gag-eGFP) or
229 intermediate cleavage products (Figure 5D). CA-eGFP is apparently correctly processed from the
230 precursor protein and is encapsidated in the virions and our sensitive imaging system allows us to
231 detect low numbers of intra-particle CA-eGFP monomers.
232 To exclude the possibility that CA-eGFP is located outside of the viral cone, we next determined the
233 intra-particle location of CA-eGFP monomers by permeabilizing the particles with saponin (35)
234 (Figure 6A). We mounted the purified, double-labelled viruses onto slides and subjected them to a 5
235 min treatment with either PBS or saponin. Saponin punctures small holes in the viral membrane,
236 causing all proteins not stably associated with the core or embedded in it to dissociate. In the
237 absence of saponin, viral particles are intact and so both IN-mCherry and CA-eGFP should be
238 detected as clear fluorescent foci. Important to note is that such short saponin permeabilization will

Accepted Manuscript Posted Online

Journal of Virology

JVI

Journal of Virology

Downloaded from http://jvi.asm.org/ on February 4, 2020 at 26989832

not cause dissociation of HIV-1 cores, unlike treatments described elsewhere (54). As shown in Figure 6B, after PBS treatment of virus particles eGFP foci (indicative of CA-eGFP) remained intact and associated with p24 (Figure 6B, PBS panel). If CA-eGFP is monomeric and free outside of the viral core, saponin treatment should release it into the medium and the eGFP foci should disappear. Despite the loss of approximately 50% of the particles under saponin treatment (fewer detected p24 foci, possibly due to inadvertent lysis or release of p24 and CA-eGFP molecules from defective particles), eGFP foci were retained in the presence of saponin and largely colocalized with the p24 foci (Figure 6B, "saponin" panels). To determine the amount of CA-eGFP associated with the cores before and after saponin treatment, we quantified eGFP fluorescence (Figure 6C). We observe a mere 1.5-fold loss of CA-eGFP signals in saponin-permeabilized particles. These data indicate that the majority of CA-eGFP is either incorporated into or encased by the capsid core. These findings were corroborated by capsid core purification experiments, where intact cores of CA-eGFP labelled HIV particles were purified through a sucrose gradient (as described previously in 49) (Figure 6D). The core fractions were pooled, adhered to microscopic slides and stained with p24 antibody (Figure 6E). Colocalization between CA-eGFP and immunostained CA in the core fractions suggests that fluorescently labelled capsid molecules are part of the capsid cone or reside inside. We also visualized the IN-mCherry fluorescence in conditions with and without saponin (data not shown) and we observed identical profiles in both conditions, although with significant fluorescence noise as mentioned above. After this initial validation, we set out to explore our combined labelling approach for single-virus imaging.

Labelled integrase and capsid proteins display distinct intracellular distributions during early HIV transduction steps

After successful incorporation of CA-eGFP into HIV-1 particles, we next investigated whether CA-eGFP could be detected in transduced host cells and how its distribution correlated with that of IN-mCherry complexes. We used HeLaP4 cells for single virus imaging because the cytoplasm to nucleus

Accepted Manuscript Posted Online

Journal of Virology

JVI

Journal of Virology

Downloaded from http://jvi.asm.org/ on February 4, 2020 at 26989832

volume ratio is large enough to reliably localize fluorescent virus complexes to either the cytosol, the nuclear envelope (NE) or nucleus and to study the requirements of HIV-1 nuclear import (reviewed in 1, 45). HeLaP4 cells were transduced with single- or double-labelled virions for 6 h and then fixed and stained to identify the nuclear lamina (Figure 7A). Using in-house Matlab routines, we determined the numbers and fluorescence intensities of IN-mCherry and/or CA-eGFP complexes in the cytoplasm, at the NE and in the nucleus as three main compartments (Figure 7 and Table 1).

As shown in Figure 7, nuclear import of all labelled viral complexes was detected at 6 h post transduction (Figure 7B and D). Consistently with previous data (33), at this moment approximately 15% and 5% of all IN-mCherry containing PICs were detected at the NE and in the nucleus, respectively (Figure 7B and Table 1A). The IN-mCherry distribution was comparable between single- and double-labelled virions, indicating that CA-eGFP labelling does not interfere with the nuclear import of PICs labelled with fluorescent IN. The data were largely comparable among the viruses, except that particles with a higher CA-eGFP content (CA-eGFP 1:2) were impaired by 50% for nuclear import (Figure 7B and Table 1B). This correlates well with the lower transduction efficiency of these recombinant virions (Figure 4C).

While most IN-mCherry complexes was in the cytosol at 6 h, the intracellular distribution of the CA-eGFP containing complexes was markedly different (compare Figure 7B and D). Unlike the labelled IN, 80% of all CA-eGFP complexes distributed equally between the cytosol and the nuclear envelope and the remaining 20% were detected in the nucleus (Figure 7D).

In addition to the localization profiles, we also determined fluorescence intensities of the viral complexes (Figure 7C and E). Nuclear IN-mCherry complexes had a significantly lower intensity compared to their cytosolic counterparts, confirming previous findings (33) on reduced IN content of nuclear PICs (Figure 7C). In striking contrast, no significant change in CA-eGFP fluorescence intensities between the different compartments was seen (Figure 7E). Note that any loss of CA-eGFP from the core and/or the viral PIC would result in “invisible” capsid complexes, due to the low level of CA-eGFP molecules (median n = 2) per particle. Our data imply that either intact capsid cores gain

Accepted Manuscript Posted Online

Journal of Virology

JVI

Journal of Virology

Downloaded from http://jvi.asm.org/ on February 4, 2020 at 26989832

291 access into the nucleus if CA-eGFP is a measure of overall CA or that the few CA-eGFP monomers
292 present inside the viral core are imported in the nucleus. While discrete changes in CA-eGFP intensity
293 could not be reliably observed, we also analyzed the fraction of high-intensity (> 1.5 a.u.) CA-eGFP
294 labelled particles in the three main intracellular compartments (cytosol, nuclear envelope, nucleus)
295 (Figure 7F). This type of analysis included the complexes equivalent to the top 15% highest intensity
296 cytosolic CA-eGFP complexes. We observed a higher fraction of these bright CA-eGFP foci in the
297 cytosol compared to the NE and the nucleus, indicating that part of CA-eGFP is lost from PICs while
298 trafficking from the cellular to nuclear membrane or that PICs with a higher CA-eGFP content,
299 perhaps also in the cone, do not make it into the nucleus.
300 The difference in relative fluorescent PIC distribution may point to differences in the dynamics of
301 nuclear import between the labelled capsid and integrase complexes. This notion is also supported
302 by the data obtained on complexes containing both IN-mCherry and CA-eGFP (Figure 7G). At 6 h post
303 infection, between 18% and 23% of all cytosolic IN-mCherry complexes contain CA-eGFP, whereas
304 this colocalization rate drops to 15% at the nuclear envelope and to 7% in the nucleus. The largest
305 difference between IN-mCherry and CA-eGFP distribution was observed at the NE (compare Figure 7
306 panels H and I). The percentage of IN-mCherry complexes containing CA-eGFP dropped only slightly
307 between cytosol and the NE (Figure 7H) in contrast to CA-eGFP complexes where the fraction
308 colocalizing with IN-mCherry was four-fold reduced at the nuclear envelope (Figure 7I). Most capsid
309 complexes are probably associated with the non-functional viral core remnants resulting from
310 uncoating and the release of IN-mCherry labelled PICs. At 6 h post infection, 15% of labelled
311 integrase complexes at the nuclear envelope still contain CA-eGFP, which may point to PICs docked
312 at the NE. The remaining IN-mCherry complexes docked at the NE are likely derived from either
313 completely uncoated complexes or those containing unlabelled capsid. We previously demonstrated
314 by fluorescence microscopy of eGFP-IN labelled virus, that almost half of IN molecules dissociate at
315 this stage, explaining the presence of eGFP-IN outside the nucleus (33). Only 3% of CA-eGFP
316 complexes in the nucleus contained IN-mCherry even though the labelling of IN is more efficient. The

Accepted Manuscript Posted Online

Journal of Virology

JVI

Journal of Virology

Downloaded from http://jvi.asm.org/ on February 4, 2020 at 26989832

317 modest particle CA-eGFP labelling efficiency of 25-30% may contribute to an apparently low extent of
318 nuclear CA-eGFP and IN-mCherry colocalization. The data indicate that dissociation of CA-eGFP from
319 IN-mCherry complexes likely occurs at the NE.
320 As indicated by a relatively high (20%) percentage of CA-eGFP complexes in the nucleus, it is possible
321 that CA-eGFP complexes are imported into the nucleus either alone or in association with viral PICs,
322 but quickly dissociate from them upon nuclear entry. Either way, the presence of free nuclear CA-
323 eGFP implies that CA may play a role unrelated to integration. Alternatively, CA-eGFP dissociated
324 from the PIC may be degraded in the nuclear proteasome.
325 Control experiments confirmed that the fluorescent complexes detected were derived from fusion
326 competent viruses (Figure 8). When we used virus-like particles without VSV-G envelope in parallel
327 with enveloped viruses to transduce HeLa P4 cells, two- to 10-fold fewer IN-mCherry and CA-eGFP
328 complexes were observed in the cytoplasm, at the NE and no complexes were detected in the
329 nucleus (Figure 8 and Table 2). The data were consistent regardless of the time of cell fixation (1.5 h
330 or 6 h post infection) (Figure 8A and Figure 8B, respectively).
331 For further experiments we focused on CA-eGFP 1:10 particles since CA-eGFP 1:2 displayed a partially
332 defective nuclear import of IN-mCherry labelled PICs (Figure 7A) and impaired transduction
333 efficiency.
334
335 **IN-mCherry and CA-eGFP labelled complexes belong to a functional virus pool**
336 In order to confirm that our approach ensures labelling of functional particles, we investigated the
337 distribution of fluorescent viral complexes after treatment with PF74, a capsid-binding HIV-1 inhibitor
338 (Figures 9 and 10). We transduced HeLaP4 cells with single- or double-labelled virions in the presence
339 of either DMSO (vehicle control) or PF74 (2 µM and 10 µM) (Figure 9 and 10). The inhibitory effect of
340 PF74 was tested at both early (1.5 h) and late (6 h) time points post infection.
341 At 1.5 h post transduction, PF74 did not exhibit any influence on the intracellular distribution of IN-
342 mCherry containing complexes (Figure 9B and Table 3A). While the lower (2 µM) PF74 concentration

Accepted Manuscript Posted Online

Journal of Virology

JVI

Journal of Virology

Downloaded from http://jvi.asm.org/ on February 4, 2020 at 26989832

343 was not expected to alter IN-mCherry distribution, it was somewhat surprising to observe no effect
344 on the presence of IN-mCherry complexes at the nuclear envelope in the presence of 10 µM PF74.
345 However, this may be a sensitivity issue, as only low numbers of IN-mCherry PICs are observed at the
346 NE soon after infection.
347 We next analyzed early effects of PF74 on CA-eGFP containing complexes. In the presence of the
348 DMSO control, docking to the nuclear envelope and nuclear import was observed for CA-eGFP
349 complexes as early as 1.5 h after infection (Figure 9C). In contrast to IN-mCherry, labelled capsid
350 complexes were unable to dock at the nuclear envelope in the presence of high (10 µM) PF74
351 concentration and their nuclear import was blocked by both 2 µM and 10 µM PF74 (Figure 9C and
352 Table 3B). These data agree with previous studies, describing capsid perturbation and inhibition of
353 nuclear import by PF74 (23, 28, 33, 36). Importantly, the inhibition of CA-eGFP docking to the NE by
354 10 µM PF74 indicates that these complexes are part of a functional virion pool.
355 We next assessed PF74 inhibition at 6 h post transduction (Figure 9D and E and Table 4). The
356 intracellular distribution of CA-eGFP complexes in the presence of DMSO was slightly different
357 compared to the initial experiment, as the percentage of CA-eGFP in the nucleus was increased.
358 However, the overall CA-eGFP distribution was reproducible between experiments. Two µM PF74
359 potently inhibited nuclear import of both IN-mCherry and CA-eGFP containing complexes, (Figure 9D
360 and E, respectively; Table 4) and 10 µM PF74 abolished the localization of IN-mCherry and CA-eGFP
361 PICs at the nuclear envelope (Figure 9D and E; Table 4). Decreased complex numbers detected under
362 high PF74 concentration agree with the capsid destabilizing effect of this inhibitor concentration (27).
363 In addition to the absolute numbers of fluorescent viral complexes, we also probed their content in
364 the absence versus the presence of inhibitor (Figure 10; Tables 3 and 4). At 1.5 h post infection, 10
365 µM induced a small, yet statistically significant increase in fluorescence intensity of cytoplasmic IN-
366 mCherry complexes (1.35- and 1.19-fold increase for WT-mCh and CA-eGFP 1:10 infections,
367 respectively) (Figure 10A). There was no significant change in the content of CA-eGFP complexes
368 (Figure 10B). At 6 h post infection, treatment with 10 µM PF74 also induced increased fluorescence

Accepted Manuscript Posted Online

Journal of Virology

JVI

Journal of Virology

Downloaded from http://jvi.asm.org/ on February 4, 2020 at 26989832

intensities of cytoplasmic and NE IN-mCherry complexes (Figure 10C). For complexes detected in WT-mCh condition, fluorescence intensity was 0.95-fold decreased in the cytosol, but 1.24-fold increased at the nuclear envelope. For the CA-eGFP 1:10 condition, fluorescence intensities of IN-mCherry were 1.12- and 1.24-fold increased in the cytoplasm and at the NE under the same PF74 treatment. PF74 is not expected to directly affect IN-mCherry content of the viral PICs and the effects of high PF74 concentration, although statistically significant, are discrete. One possibility is that IN-mCherry fluorescence is detected more efficiently when the cone is destabilized by high PF74. As for the CA-eGFP intensity profiles, the data should be interpreted cautiously due to the low numbers of encapsidated CA-eGFP monomers. The CA-eGFP content in the viral complexes was unaffected by PF74 treatment at 1.5 h post infection (Figure 10B). In contrast, the CA-eGFP intensity was significantly increased by 2 µM PF74 for cytoplasmic and NE complexes (1.33- and 1.37-fold increase, respectively) detected at 6 h post infection (Figure 10D). These data agree with previous findings on capsid-stabilization effects of low PF74 concentrations, whereby CA-eGFP fluorescence possibly increases due to aborted or delayed uncoating and associated loss of some CA-eGFP molecules. The finding that 10 µM PF74 does not radically influence the CA-eGFP content (Figure 10B and D) further supports the hypothesis that this fusion protein is not part of the core surface and resides solely inside the core and not in a hexameric form.

As an additional confirmation that the visualized complexes originate from fusion-competent particles, we compared fluorescence intensities of intact viruses spotted on coverslips and post-fusion viral complexes, identified in the target cells (Figure 10E and 10F). The fluorescence intensities of both cytoplasmic IN-mCherry and CA-eGFP complexes are lower compared to the intact viruses used for transduction and imaged under the same conditions. We hence conclude that the observed and analyzed viral complexes derive from fusion-competent virus particles.

To corroborate our imaging data, we performed transduction experiments in the presence of DMSO or PF74 to quantify luciferase reporter gene expression and viral DNA species in infected HeLa P4 cells (Figure 11). To compare the transduction efficiency of unlabelled, single- and dually-labelled

Accepted Manuscript Posted Online

Journal of Virology

JVI

Journal of Virology

Downloaded from http://jvi.asm.org/ on February 4, 2020 at 26989832

viruses, we transduced HeLaP4 cells in parallel with different dilutions of virus after initial normalization for p24. As shown in Figure 11A, transduction efficiencies were comparable between all viruses, confirming that IN-mCherry and/or CA-eGFP co-labelling do not drastically interfere with transduction. PF74 inhibited transduction of all viruses in a concentration-dependent manner (Figure 11A). We also quantified total viral DNA after normalization for cellular genomic DNA content (Figure 11B). Viral integration was evaluated only in the absence of inhibitor and integration rates (measured by the Gag gene levels in the cellular genomic DNA) were comparable for all viruses (Figure 11B, bottom panel).

Presence of CA-eGFP in the nucleus

Previously, our lab showed that IN-FP labelling enables visualization of functional viral complexes in target cells (33). A hallmark feature of IN-FP functionality is the observed accumulation of fluorescent IN complexes in the nucleus upon addition of the integrase strand transfer inhibitor raltegravir (RAL) (33), which was recently confirmed in an independent study (18). Here we asked how RAL influences intracellular distributions of CA-eGFP complexes at 6 h post infection. We first analyzed IN-mCherry distribution profiles and detected that, like IN-eGFP, the mCherry-tagged IN complexes accumulated in the nucleus upon integrase inhibition (Figure 12A). This accumulation was observed as a significantly increased percentage of nuclear complexes compared to the total number of intracellular IN-mCherry complexes. The percentage of CA-eGFP complexes in the nucleus was unaffected by RAL addition (Figure 12B). Next, we quantified the percentages of single- (CA-eGFP or IN-mCherry) and double-labelled (IN-mCherry + CA-eGFP) complexes in the nucleus of cells infected with double-labelled virions (CA-eGFP 1:10) (Figure 12C-E). Interestingly, inhibiting integration resulted in distinct effects on double-labelled viral complexes. When plotting percentages of nuclear IN-mCherry complexes per cell (Figure 12C) in cells infected with double-labelled virions, we observed that the percentage of IN-mCherry-only containing complexes was increased upon RAL treatment, while there was no effect on the accumulation of double-labelled complexes (Figure 12C

Accepted Manuscript Posted Online

Journal of Virology

JVI

Journal of Virology

Downloaded from http://jvi.asm.org/ on February 4, 2020 at 26989832

421 and E). We then plotted the percentages of CA-eGFP complexes, containing either only the tagged CA
422 or both labelled CA and IN (Figure 12D and E). We observed no significant changes in the percentages
423 of either complex species, relative to the total number of intracellular CA-eGFP complexes. These
424 data indicate that the majority of CA-eGFP containing complexes either may not belong to
425 integration competent PICs or that capsid (and CA-eGFP) must dissociate prior to generation of
426 integration competent PICs. In agreement with previous studies, it is possible that the PIC associated
427 CA and CA-eGFP influence nuclear import, migration and/or targeting of PICs inside the nucleus, but
428 that they are likely not involved in the integration reaction.
429
430 **Discussion**
431 In this study, we describe an original HIV-1 capsid protein labelling strategy using CA-eGFP. Using an
432 extended confocal imaging platform for HIV-1, we show that: (1) low amounts of eGFP-labelled CA
433 protein are incorporated into virus particles without major interference with viral transduction or
434 nuclear import of IN-mCherry labelled PICs; (2) CA-eGFP is located inside the viral capsid core; (3) CA-
435 eGFP containing virions belong to a functional virus pool; (4) Nuclear CA-eGFP containing IN
436 complexes respond differently to integrase inhibitors than complexes without (the labelled) CA.
437 Taken together, these data highlight the validity of our labelling system and the use of CA-eGFP as a
438 direct marker of a functional capsid protein pool.
439 Following the fate of HIV-1 CA in infected cells has gained increasing interest in recent years, as the
440 possible role of this protein in post-uncoating steps attracted much attention and controversy
441 (reviewed in 1). Previous studies pointed to important roles for CA in docking of HIV-1 PICs to the NE
442 and their consecutive import into the nucleus (reviewed in 1). The CA protein itself was detected in
443 the nucleus, albeit predominantly using immunostaining with specialized protocols (24, 25).
444 Therefore, we opted for developing a direct CA labelling strategy, to allow robust detection of this
445 viral protein in the nucleus and to decipher its intracellular distribution with respect to IN-FP labelled
446 viral PICs.

Accepted Manuscript Posted Online

Journal of Virology

JVI

Journal of Virology

Downloaded from http://jvi.asm.org/ on February 4, 2020 at 26989832

447 In our strategy, we produce transduction competent particles containing an excess of untagged over
448 tagged CA. We postulate that the CA-eGFP protein is located primarily inside mature virus cores.
449 Following lines of evidence support this model. i) The particles incorporate on average only 2 CA-
450 eGFP monomers per virion (Figure 5C); ii) tagged CA molecules are resistant to saponin-mediated
451 membrane stripping in vitro, excluding CA-eGFP location in between the viral core and membrane
452 (Figure 6A-B); iii) Fluorescence intensity measurements point to the relatively unaltered CA-eGFP
453 signal from entry to nuclear import, which can be explained by a few CA-eGFP monomers that reside
454 inside the cone and that are therefore unaffected by uncoating (Figure 7E). We believe that our
455 approach visualizes an insufficiently discussed intraparticle CA population, which is present inside the
456 viral core and associates with the viral PICs during early infection. Of course, at this stage we cannot
457 exclude that eGFP tagging of CA may have artificially resulted in this CA population. Since CA-eGFP is
458 present only in approximately 25-30% of all virus particles (Figure 5B), we admit that this labelling is
459 less efficient compared to some previously published approaches, such as binding of CypA-dsRed to
460 viral cores (35) or tC tagging of CA in recombinant virions (37, 38). However, a considerable
461 advantage of using CA-eGFP compared to those approaches is the direct visualization of CA, rather
462 than its interacting partner (in the case of CypA-dsRed) or the use of a secondary dye (such as FlAsH;
463 in the case of tC labelling). Additionally, CA-eGFP offers a good alternative to CA immunostaining
464 approaches, which provide a limited and variable visualization of CA in the host cell nucleus and are
465 not suited for live-cell imaging approaches (23-25).
466 Importantly, CA-eGFP complexes represent functional complexes, as illustrated by the following
467 experiments: i) the number of CA-eGFP complexes derived from VLPs is significantly lower than from
468 enveloped particles and they are deficient for nuclear import (Figure 8); ii) PF74 prevents nuclear
469 envelope docking and nuclear import of CA-eGFP complexes in a dose-dependent manner (Figure 9),
470 consistently with previous findings (23, 29).
471 While CA-eGFP present within the viral cone cannot be used as a direct label for core uncoating, it
472 may provide a useful tool for labelling and tracking of the functional CA population. Low PF74

Accepted Manuscript Posted Online

Journal of Virology

JVI

Journal of Virology

Downloaded from http://jvi.asm.org/ on February 4, 2020 at 26989832

473 concentrations do not cause capsid destabilization (23, 25, 29), but may still perturb the uncoating
474 process and thereby prevent HIV-1 nuclear import. In agreement with this model, 2 µM of PF74
475 blocked the nuclear import of both CA-eGFP and IN-mCherry complexes. Consistently with previous
476 studies, 10 µM PF74 also inhibited docking of both CA-eGFP and IN-mCherry particles at the nuclear
477 envelope, which in turn is consistent with the NE uncoating model (see Figure 13 for summary). An
478 additional observation that supports this model in our study is the low colocalization rate of IN-
479 mCherry and CA-eGFP at the NE. Even though CA-eGFP may reside within the core, uncoating or a
480 post-uncoating CA rearrangement would be required to free it from IN-mCherry. Due to the presence
481 of many free CA-eGFP complexes (approximately 95% of all CA-eGFP complexes) at the NE and in the
482 nucleus, we propose a model in which the majority of labelled capsid and integrase proteins are
483 independently imported into the nucleus and likely perform distinct roles there.
484 The present data on CA-eGFP distribution largely agree with previous publications, which imply the
485 existence of capsid multimers that persist after uncoating and nuclear import (18, 24-25). As even
486 from dynamic studies it is unclear which CA rearrangements occur during uncoating (18), these
487 complexes may have been released from PICs together with viral core remnants at the moment of
488 nuclear import. The presence of CA-eGFP in the nucleus is in line with previous findings, describing
489 relatively low capsid protein content in the nucleus of infected cells (18, 25). Even though it has
490 previously been shown that the intensity of immunostained or otherwise labelled CA complexes is
491 five- to 10-fold lower than in the cytoplasm (18, 25), it is possible to detect them as clear foci
492 indicating that nuclear CA exists in a multimeric form.
493 Once localized in the nucleus, 97% of CA-eGFP complexes do not contain IN-mCherry and do not
494 seem to participate in integration, as deduced from our RAL experiments (Figure 12B and D).
495 Accumulation of IN-mCherry complexes under RAL treatment is particularly clear when comparing
496 PICs that contain only labelled IN and those that contain both IN-mCherry and CA-eGFP (Figure 12C).
497 The percentage of PICs containing only IN significantly increases by approximately 50%, while the
498 population of double-labelled complexes remains unchanged. In contrast to these data, analysis of

Accepted Manuscript Posted Online

Journal of Virology

JVI

Journal of Virology

Downloaded from http://jvi.asm.org/ on February 4, 2020 at 26989832

499 CA-eGFP containing nuclear complexes revealed a different phenotype (Figure 12B and D). No effect
500 was seen on the overall percentage of CA-eGFP complexes (both without and with IN-mCherry) in the
501 nucleus (Figure 12B and D). Our data indicate that most nuclear CA complexes differ from IN
502 complexes without CA in response to integrase inhibitors suggesting that the labelled CA complexes
503 do not participate in integration. We believe our data add value to previous studies, mostly due to
504 their quantitative aspect. Previously, Chin and colleagues (24) implied that CA is associated with
505 integration competent virus complexes in the nucleus, based on the observed stabilization of CA
506 colocalization with vDNA under RAL treatment, but without any detailed quantification. These data
507 were more recently challenged by another study (18), which showed that integration events (marked
508 by IN-eGFP disappearance in the nucleus) did not contain CA in 50% of the cases. Our data thus agree
509 with the latter findings and with a recently published study (51), whereby the primary role of nuclear
510 CA is in traversing the nuclear lamina to allow PICs to reach optimal regions prior to integration.
511 Our present imaging analysis confirms previous findings on integration- competent PICs in the
512 nucleus (33) but leaves ground for future mechanistic studies. To expand these findings on the role of
513 CA and CA-eGFP inside the nucleus, a time-course analysis of integration-deficient virus and/or
514 mutants not interacting with CPSF6 (such as N74D and A77V) is planned. It will also be interesting to
515 perform integration site analyses of cells transduced with single- and double-labelled viruses. Future
516 live-cell imaging studies will shed further light on these events. Taken together, our capsid labelling
517 system enables tracking of functional virus particles and therefore represents a relevant
518 complementary system to the existing methodologies for further dissecting the role of HIV-1 capsid
519 during early infection.
520
521 **Materials and Methods**
522
523 **Cells**

524 All mammalian cell lines were cultured at 37 °C in a humidified atmosphere with 5% CO_2. HeLa P4 (a
525 kind gift from Dr. Pierre Charneau, Institut Pasteur, Paris, France) and HEK293T (ATCC CRL-11268)

Accepted Manuscript Posted Online

Journal of Virology

JVI

Journal of Virology

Downloaded from http://jvi.asm.org/ on February 4, 2020 at 26989832

526 cells were maintained in Dulbecco's modified eagle medium (DMEM, Life Technologies Europe,
527 Merelbeke, Belgium) supplied with 5% (v/v) fetal calf serum (FCS) and 50 µg/ml gentamycin (Life
528 Technologies) and, in the case of HeLa P4 additionally 500 µg/ml geneticin (Gibco BRL). The cells
529 were subcultured twice a week.

530 **Recombinant DNA**

531 The pNL4-3.Luc.R-E- construct was obtained through the NIH AIDS Reagent program (catalog number
532 #3418) from Dr. Nathaniel Landau (39). The plasmid pVpr-IN-eGFP was described previously (32) and
533 pVpr-IN-mCherry was constructed by replacing the eGFP gene in pVpr-IN-eGFP with mCherry via
534 *BamHI*/*NotI* restriction sites. The linker between IN and the FP is the same in both constructs. pLP-
535 VSV-G was described previously (pLP-VSVG #646 B, Invitrogen). Two types of tC tags were used for tC
536 tagging of CA: the shorter (CCPGCC, inserted within the CA sequence) and longer tC tag
537 (FLNCCPGCCMEP, attached at the N- or C-terminus of CA). Site-directed ligase independent
538 mutagenesis (SLIM) method (53) was used to introduce the corresponding tC CA tags into pNL4-
539 3.Luc.R-E-. Each primer used in the SLIM approach is annotated by its orientation (F- forward, sense;
540 R- reverse, antisense) and special feature (t-tailed; s-short). The pNL4-3.Luc.R-E- based constructs
541 coding for tC tagged CA variants (thus named pNL4-3.Luc.R-E- tC) and primers used were the
542 following: tC_{4-9} (Ft- TGGTACATCAGGCCATATCACC; Fs-
543 TGTTGTCCCGGGTGTTGCATGGTACATCAGGCCATATCACC; Rt- CACTATAGGGTAATTTTGGCTGACC; Rs-
544 TGCAACACCCGGGACAACACACTATAGGGTAATTTTGGCTG ACC), tC_{91-95} (Ft-
545 ATGAGAGAACCAAGGGGAAGTG; Fs- TGTTGTCCAGGATGTTGTATGAGAGAACCAAGGGG AAGTG; Rt-
546 AGGCCCTGCATGCACTGG; Rs- ACAACATCCTGGACAACAAGGCCCTGCATGCACTGG), $tC_{120-124}$ (Ft-
547 CAGTAGGAGAAATCTATAAAAGATGG; Fs- TGTTGCCCAGGATGTTGTCCAGTAGGAGAAATCTATAAAAG
548 ATGG; Rt- TGTCATCCATCCTATTTGTTCC; Rs- GACAACATCCTGGGCAACATGTCATCCATCCTATTTGTTCC),
549 $tC_{206-210}$ (Ft- CTAGAAGAAATGATGACAGC; Fs- TGTTGTCCCGGGTGTTGTCTAGAAGAAATGAT GACAGC;
550 Rt-CAATGCTTTTAAAATAGTCTTACAATC; Rs-

Accepted Manuscript Posted Online

ACAACACCCGGGACAACACAATGCTTTTAAAATAGTCTTACAA TC), tC-CA (N-terminal fusion) (Ft- CCTATAGTGCAGAACCTCCAGG; Fs- CCAATTGTGCAGTTTCTGAATTGT TGTCCCGGGTGTTGTATGGAACCTCCTATAGTGCAGAACCTCCAGG; Rt- GTAATTTTGGCTGACCTGGCTG; Rs- AGGTTCCATACAACACCCGGGACAACAATTCAGAAACTGCACAATTGGGTAATTTTGGCTGACCTGGCTG) and CA-tC (C-terminal fusion) (Ft- GCTGAAGCAATGAGCCAAG; Fs- TTTCTGAATTGTTGTCCCGGGTGTTG TATGGAACCTGCTAGGGTGCTAGCTGAAGCAATGAGCCAAG; Rt- CAAAACTCTTGCTTTATGGCCG; Rs- TAG CACCCTAGCAGGTTCCATACAACACCCGGGACAACAATTCAGAAACAAAACTCTTGCTTTATGGCCG). N- and C-terminal eGFP tagging of CA was achieved by ligating the *BamHI/SpeI*- and *SpeI/ApaI* digested gBlocks (IDT, Leuven) into the pNL4-3.Luc.R-E- backbone respectively. The construct pNL4-3.Luc.R-E-CA-eGFP (referred to as NL4-3 Luc CA-eGFP) is a modification of the above vector though replacement of the capsid sequence in the *gag* ORF with the CA-eGFP fusion sequence.

Full gBlock sequence for eGFP-CA fusion (*Italic underlined* – Duplicated protease cleavage site; *Italic* - eGFP; Underlined – GGSGT linker; **Bold** - N-terminus of CA; **ACTAGT** – SpeI restriction site)

GAGTTAATACGACTCACTATAGGGGGATCCGAAGAACTTAGATCATTATATAATACAATAGCAGTCCTCTATTG
TGTGCATCAAAGGATAGATGTAAAAGACACCAAGGAAGCCTTAGATAAGATAGAGGAAGAGCAAAACAAAA
GTAAGAAAAAGGCTCAGCAAGCAGCAGCTGACACAGGAAACAACAGCCAGGTC*AGCCAAAATTACCCCATCG*
*TACAAAAT*ATGGTGAGCAAGGGCGAGGAGCTGTTCACCGGGGTGGTGCCCATCCTGGTCGAGCTGGACGGCG
ACGTAAACGGCCACAAGTTCAGCGTGTCCGGTGAGGGGGAGGGCGACGCAACTTATGGCAAATTGACGCTCA
AGTTTATCTGCACCACAGGCAAGCTTCCCGTGCCCTGGCCTACATTGGTGACCACTCTGACTTACGGGGTGCAG
TGT TTCAGTAGAT ATCCCGACCACATGAAGCAGCACGATTTCTTCAAGAGTGCAATGCCCGAAGGTTACGTAC
AGGAAAGGACTATTTTCTTCAAGGACGATGGTAACTATAAAACTCGGGCGGAGGTGAAATTCGAGGGGGACA
CGCTGGTAAATCGCATTGAGCTGAAGGGAATCGATTTCAAAGAGGATGGCAATATCCTCGGCCATAAATTGGA
ATACAACTATAACAGTCATAATGTGTACATTATGGCAGACAAGCAGAAAAACGGGATAAAAGTCAATTTCAAG
ATTAGACATAACATAGAAGATGGGTCAGTCCAGCTCGCAGATCACTATCAGCAGAACACACCCATTGGGGATG
GACCAGTGCTGCTCCCTGACAACCACTACCTGAGCACCCAGTCCGCCCTGAGCAAAGACCCCAACGAGAAGCG
*CGATCACATGGTCCTGCTGGAGTTCGTGACCGCCGCCGGGATCACTCTCGGCATGGACGAGCTGTACAAG*GGA

Downloaded from http://jvi.asm.org/ on February 4, 2020 at 26989832

Journal of Virology JVI Journal of Virology

Accepted Manuscript Posted Online

Journal of Virology

JVI

Journal of Virology

GGGTCCGGAACA**CCTATAGTGCAGAACCTCCAGGGGCAAATGGTACATCAGGCCATATCACCGCGGACTTTA**
AATGCATGGGTAAAAGTAGTAGAAGAGAAGGCTTTCAGCCCAGAAGTAATACCCATGTTTTCAGCATTATCA
GAAGGAGCCACCCCACAAGACCTAAATACCATGCTAAACACAGTGGGGGGACATCAAGCAGCCATGCAAAT
GTTAAAAGAGACCATCAATGAGGAAGCTGCAGAATGGGATAGATTGCATCCAGTGCATGCAGGGCCTATTG
CACCAGGCCAGATGAGAGAACCAAGGGGAAGTGACATAGCAGGAACTACTAGTCCGCTGAGCAATAACTAG
CCTGA

Full gBlock sequence for CA-eGFP fusion (**Bold** - CA C-terminus; **ACTAGT** - SpeI restriction site; **ACAAGCAT** - mutated BstxI site; underlined - DPPVAT linker; *Italic*- eGFP*)*:

GAGTTAATACGACTCACTATAGGG**ACTAGTACCCTTCAGGAACAAATAGGATGGATGACACATAATCCACCT**
ATCCCAGTAGGAGAAATCTATAAAAGATGGATAATCCTGGGATTAAACAAAATAGTAAGAATGTATAGCCC
T*ACAAGCATT*CTGGACATAAGACAAGGACCAAAGGAACCCTTTAGAGACTATGTAGACCGATTCTATAAAAC
TCTAAGAGCTGAGCAAGCTTCACAAGAGGTAAAAAATTGGATGACAGAAACCTTGTTGGTCCAAAATGCGA
ACCCAGATTGTAAGACTATTTTAAAAGCATTGGGACCAGGAGCGACACTAGAAGAAATGATGACAGCATGT
CAGGGAGTGGGGGGACCCGGCCATAAAGCAAGAGTTTTGGATCCTCCAGTGGCCACC*ATGGTGAGCAAGGG*
CGAGGAGCTGTTCACCGGGGTGGTGCCCATCCTGGTCGAGCTGGACGGCGACGTAAACGGCCACAAGTTCAG
CGTGTCCGGTGAGGGGGAGGGCGACGCAACTTATGGCAAATTGACGCTCAAGTTTATCTGCACCACAGGCAA
GCTTCCCGTGCCCTGGCCTACATTGGTGACCACTCTGACTTACGGGGTGCAGTGTTTCAGTAGATATCCCGACC
ACATGAAGCAGCACGATTTCTTCAAGAGTGCAATGCCCGAAGGTTACGTACAGGAAAGGACTATTTTCTTCAAG
GACGATGGTAACTATAAAACTCGGGCGGAGGTGAAATTCGAGGGGGACACGCTGGTAAATCGCATTGAGCTG
AAGGGAATCGATTTCAAAGAGGATGGCAATATCCTCGGCCATAAATTGGAATACAACTATAACAGTCATAATG
TGTACATTATGGCAGACAAGCAGAAAAACGGGATAAAAGTCAATTTCAAGATTAGACATAACATAGAAGATGG
GTCAGTCCAGCTCGCAGATCACTATCAGCAGAACACACCCATTGGGGATGGACCAGTGCTGCTCCCTGACAACC
ACTACCTGAGCACCCAGTCCGCCCTGAGCAAAGACCCCAACGAGAAGCGCGATCACATGGTCCTGCTGGAGTT
*CGTGACCGCCGCCGGGATCACTCTCGGCATGGACGAGCTGTACAAG*GCCCGGGTACTGGCTGAAGCAATGAG
CCAAGTAACAAATCCAGCTACCATAATGATACAGAAAGGCAATTTTAGGAACCAAAGAAAGACTGTTAAGTGT
TTCAATTGTGGCAAAGAAGGGCACATAGCCAAAAATTGCAGGGCCCCCGCTGAGCAATAACTAGCCTGA

Downloaded from http://jvi.asm.org/ on February 4, 2020 at 26989832

Accepted Manuscript Posted Online

Journal of Virology

JVI

Journal of Virology

Downloaded from http://jvi.asm.org/ on February 4, 2020 at 26989832

603

604 **Virus particle production**

605 Recombinant, replication-deficient HIV-1 particles were produced by transient transfection of
606 selected plasmids into 293T cells, as described previously (33). The plasmid mixtures consisted of 15
607 µg NL4-3 Luc –based construct (either pNL4-3.Luc.R-E- only or mixed at 2:1 and 10:1 ratios with
608 pNL4-3 Luc CA-eGFP), 15 µg pVpr-IN-eGFP or pVpr-IN-mCherry and 5 µg pVSV-G plasmid per 10 cm
609 cell culture dish unless explicitly stated otherwise. For production of unlabelled virus particles, 15 µg
610 of pNL4-3.Luc.R-E- construct was cotransfected with 5 µg of pLP-VSV-G plasmid. Transfection was
611 mediated by branched polyethyleneimine (bPEI, Sigma-Aldrich) and medium was changed to fresh
612 OptiMEM (Life technologies) medium with 50 µg/ml gentamycin 6 h post transfection. Virus particles
613 were harvested 48 h after transfection, by passing the supernatants through a 0.45 µm pore filter
614 (Sartorius) and concentrating them via ultracentrifugation in a Beckman (Beckman Coulter, Ireland)
615 SW28 rotor at 133,000 x *g*, for 1.5 h at 21 °C atop a 60% (w/v) Optiprep iodixanol (Sigma-Aldrich)
616 gradient cushion. Residual Optiprep was removed by a series of washing steps (in serum-free
617 OptiMEM medium) and virus particles were concentrated by ultrafiltration (Vivaspin columns,
618 MWCO 50K, Belgium).

619

620 **Virus quantification**

621 Virus production efficiency was quantified by measuring the levels of HIV-1 capsid (p24) protein by
622 ELISA (INNOTEST p24-ELISA, Innogenetics, Gent, Belgium) or by measuring the reverse transcriptase
623 (RT) activity of particles present in the supernatant. p24 ELISA was performed according to
624 manufacturer's instructions and RT activity was assessed by a qPCR based, SYBR Green product-
625 enhanced RT (SG-PERT) assay (40, 41).
626 The SG-PERT assay quantifies the cDNA reverse transcribed from an exogenous MS2 RNA template
627 by the virus particle associated HIV-1 RT. Viruses were lysed for 5 min (0.125% Triton X-100, 25 mM
628 KCl, 50 mM Tris-HCl pH 7.4, 20% (v/v) glycerol, 0.2 U/µL RNase inhibitor in Milli-Q (Ribolock,

Accepted Manuscript Posted Online

Journal of Virology

JVI

Journal of Virology

Downloaded from http://jvi.asm.org/ on February 4, 2020 at 26989832

629 ThermoFisher Scientific)) and diluted ten-fold in sample dilution buffer (5 mM $(NH_4)_2SO_4$, 20 mM KCl,
630 20 mM Tris-HCl pH 8.3). The qPCR reaction mix consisted of 2.5 mM $(NH_4)_2SO_4$, 10 mM KCl, 10 mM
631 Tris-HCl pH 8.3, 5 mM $MgCl_2$, 0.1 mg/mL BSA, 1/5000 SYBR green I (ThermoFisher Scientific), 250 µM
632 dNTPs, 2 µM sense primer 5'-TCCTGCTCAACTTCCTGTCGAG-3', 2 µM antisense primer 5'-
633 CACAGGTCAAACCTCCTAGGAATG-3', 1 µg/mL MS2 RNA (Roche) and 0.025 U/µL Truestart Hot Start
634 Taq DNA polymerase (ThermoFisher scientific). Reverse transcription of the RNA template was
635 conducted for 1 h at 37°C, followed by qPCR (to quantify the cDNA amounts), which was run on a
636 LightCycler® 480 (Roche Life Science). The qPCR program included a 5 min activation step at 95 °C
637 and 50 cycles of amplification (5 s at 95 °C, 5 s at 55 °C, 15 s at 72 °C).
638
639 **Single-cycle virus transduction assay**
640 One day prior to transduction, 15,000 HeLa P4 cells were seeded per well in 96-well plates and
641 incubated in DMEM with 5% FBS, 50 µg/ml gentamycin and 500 µg/ml geneticin (complete DMEM
642 medium). The following day, the cells were transduced with equal volumes of virus supernatant in
643 three-fold serial dilutions, starting from the highest concentration of 100 ng p24 antigen per well.
644 Medium was changed 24 h post transduction to DMEM with 5% FBS, gentamycin and geneticin and
645 the cells were incubated for additional 48 h at 37 °C. Cells were washed twice with PBS and lysed by
646 addition of lysis buffer (50 mM Tris, 200 mM NaCl, 0.2% NP40 (v/v) and 5% glycerol (v/v)). Firefly
647 luciferase (fLuc) activity was measured using fLuc assay reagent (ONE-GloTM, Promega GMBH,
648 Mannheim, Germany). Luciferase reporter levels were normalized for total protein content in each
649 well by the bicinchoninic acid (BCA) assay (BCA Protein Assay Kit, Thermo Scientific).
650
651 **Quantitative analysis of viral DNA species in transduced HeLa P4 cells**
652 Recombinant viruses were produced as described above. HeLa P4 cells were seeded at a density of 1
653 x 10^6 cells per well in a 6-well plate and transduced 24 h later with 5 µg p24 per well of the following
654 VSV-G pseudotyped HIV-1 particles: untagged (WT), IN-mCherry labelled (WT-mCh), dually-labelled

Accepted Manuscript Posted Online

(CA-eGFP 1:2 or 1:10, depending on the ratio of CA-eGFP luciferase vector to the parental NL4-3 based construct). Transductions were carried out in the presence of DMSO or PF-03450074 (PF74, 2 µM or 10 µM). For each of the qPCR quantifications, one well of cells was left untransduced (negative control, NC). Cells were harvested 7 days after transduction (p.t.) and genomic DNA was extracted using the Sigma Mammalian genomic DNA Miniprep kit (Sigma-Aldrich) according to manufacturer's instructions. We quantified integrated viral DNA copies (integrated DNA, Gag, measured 7 days p.t.). qPCR reactions were based on Bio-Rad chemistry and contained 1x iQ Supermix (Bio-Rad Laboratories), 300 nM forward primer, 300 nM reverse primer, 200 nM probe and 100 ng genomic DNA. To normalize for viral DNA copy content, we used qPCR amplification of the CCR5 gene. All qPCR reactions and analyses were conducted as described previously (33, 61, 62). All samples were run in duplicate or triplicate. Viral DNA copies were calculated based on standard curves of highly positive samples and signal backgrounds were estimated based on no-template controls. The qPCR was run on a LightCycler® 480 (Roche Life Science), including 5 min activation at 95°C and 50 cycles of amplification (10 s at 95°C followed by 30 s at 55°C).

Transduction and immunolabelling of HeLa P4 cells for single virus analysis

One day prior to transduction, 25, 000 HeLa P4 cells were seeded per well in 8-well chamber slides (Nunc Lab-Tek Chambered Coverglasses, 155411, Thermo Scientific), previously coated with poly-D-lysine (0.1 mg/ml, Sigma). The following day, cells were transduced with virus corresponding to 1-3 µg p24 antigen and fixed at indicated time points. Different viral preparations were normalized for their p24 content in order to transduce the cells with comparable amounts of virus. Briefly, the cells were washed once with PBS, incubated for 45 sec to 1 min at 37 °C in trypsin (0.25% (w/v), Life Technologies), to remove all unfused or weakly attached virus particles from the cell surface. Trypsin was inactivated by the addition of complete DMEM medium, followed by a 3 min incubation at room temperature. The cells were washed with PBS one additional time and fixed in 4% (v/v) paraformaldehyde (PFA) for 15 min at room temperature. After fixation, the cells were washed three

Journal of Virology
JVI
Journal of Virology
Downloaded from http://jvi.asm.org/ on February 4, 2020 at 26989832

Accepted Manuscript Posted Online

Journal of Virology

JVI

Journal of Virology

Downloaded from http://jvi.asm.org/ on February 4, 2020 at 26989832

times with PBS and, where indicated, stained with a lamin-specific antibody or 4',6-diamidino-2-phenylindole (DAPI). For antibody staining purposes, the cells were permeabilized 5 min with 0.1% (v/v) Triton X-100 (Sigma-Aldrich) in PBS and blocked for 30 min in blocking buffer (0.1% (v/v) Tween-20 (A4974, Applichem), 1% BSA (w/v) (Sigma-Aldrich) in PBS) at room temperature. Primary anti-lamin A/C antibody (mouse monoclonal, 1/400 dilution, sc-7292, Santa Cruz Biotechnology) was diluted in blocking buffer and incubated on cells over night at 4 °C. After extensive washing with PBS, cells were incubated in secondary anti-mouse IgG (H+L) Alexa 405 conjugate (goat polyclonal, 1/500 dilution, A-10011, Life Technologies) for 1 h at room temperature, washed and stored in PBS at 4 °C until analysis. For CA immunostaining, cells were infected with labelled viruses (see above), permeabilized and stained with anti-lamin B1 (rabbit polyclonal, 1/400 dilution, ab16048, Abcam) and anti-CA (mouse monoclonal, 1/300 dilution, AG3.0, NIH AIDS Reagent Program, Division of AIDS, NIH (Cat #4121) from Dr. Jonathan Allan) antibodies. The secondary antibodies used were anti-rabbit IgG (H+L) Alexa 405 conjugate (goat polyclonal, 1/500 dilution, A31556, Life Technologies) and anti-mouse IgG (H+L) Alexa 488 conjugate (goat polyclonal, 1/500 dilution, A-11001, Life Technologies). When DAPI staining was performed, cells were not permeabilized, but washed after PFA fixation and directly incubated in DAPI solution (5 µg/ml, 1/1000 dilution in PBS, Invitrogen) for 5 min at room temperature. The cells were then washed four times in PBS and stored in PBS at 4 °C until analysis. When DMSO or HIV-1 inhibitors were used during transduction, the cells were first pre-incubated with DMSO or inhibitor for 2 h prior to transduction. The inhibitors used were: PF74 (2 µM or 10 µM solution in DMSO, SML0835, Sigma) and RAL (0.6 µM solution in DMSO, 100 x IC_{50}, NiBSC).

Confocal microscopy and data analysis for single virus experiments

A confocal laser scanning microscope (Fluoview FV1000, Olympus, Tokyo, Japan) was used to image the target cells and virus particles. Images were acquired using the UPLSAPO 60x W NA 1.25 objective and DM405/488/559/635 polychromic excitation mirror (Olympus). Fixed cells and virus particles were imaged in 3D stacks, with a 0.3 µm step size and 4 µs/pixel sampling speed. To excite

Accepted Manuscript Posted Online

Journal of Virology

JVI

Journal of Virology

the fluorophores, the following lasers were used: a 488-nm laser for eGFP (emission collected at 505-540 nm), a 555-nm laser for mCherry (emission collected in the 575-675 nm range), a 405-nm laser Alexa Fluor 405 and DAPI (emission collected at 430-470 nm), and a 635-nm diode laser for Alexa Fluor 633 and 647 (emission collected at 655-755 nm).

Fluorescent viral complexes (IN-FP and CA-eGFP) were automatically detected, localized and their intensity was measured by an in-house MatLab routine (MathWorks Inc.), as described previously (33). Since each fluorescent complex will be smaller than the diffraction limit of the microscope, we calculated integrated intensity of each complex using the least-mean-square method after fitting the point spread function of each complex with a 2D Gaussian distribution. This was done for each z-step of the 3D image and the highest intensity (expected to be the focus point) of each complex was used for further analysis. Viral complexes were assigned to localize to either the cytoplasm, the NE or nucleus based on intensity thresholding of the stained nuclear lamin. The distances of fluorescent viral complexes to the nuclear lamin were calculated after the precise lamin fitting with a 2D Gaussian function, which was repeated in each z-slice (33).

In experiments where colocalization of two fluorescent complexes was assessed, the centroids were described as colocalizing in case they were found at a maximum of 2 pixels (206 nm) away from each other.

Data were collected from 30 individual cells corresponding to 500 - 1,000 viral complexes in each experiment. Experiments were repeated at least once, and the data are shown either from a representative experiment or as an average from two or three independent experiments. Data on individual complex numbers and their intensities are presented as individual data points under a box-plot, with 5% and 95% whiskers. The elements of each box plot represent the following: line within the box - median value, square box - mean, bar diagrams – geometric mean, error bars – back transformed standard error of the mean. P-values for the fluorescence intensity data are calculated by a two-sample t-test with unequal variance of the log-normal distributed data with the following significance criteria: p-value < 0.001 (***); $p < 0.01$ (**), $p < 0.05$ (*) and n.s. as not significant.

Downloaded from http://jvi.asm.org/ on February 4, 2020 at 26989832

Accepted Manuscript Posted Online

Journal of Virology

JVI

Journal of Virology

Downloaded from http://jvi.asm.org/ on February 4, 2020 at 26989832

Mounting and immunolabelling of virus particles for microscopy

Purified virus particles were immobilized on poly-D-lysine (0.1 mg/ml) coated 8-well chamber slides for 4 – 6 h at 37 °C, washed once with PBS and fixed with 4% PFA. After fixation, the samples were washed three times with PBS and permeabilized in 0.1% (v/v) Triton X-100 for 5 min at room temperature. Thereafter, the samples were washed twice in PBS and incubated in primary antibody (diluted in blocking buffer- 0.1% (v/v) Tween-20 (A4974, Applichem), 1% BSA (Sigma-Aldrich) in PBS) at 4 °C over night. The primary antibodies used were anti-HIV-1 CA (p24) (mouse monoclonal, 1/300 dilution, AG3.0, NIH AIDS Reagent Program, Division of AIDS, NIH (Cat #4121) from Dr. Jonathan Allan), anti-HIV-1 IN (mouse monoclonal, 1/100 dilution, IN-2 ab66645, Abcam, Cambridge, U.K.) and anti-HIV-1 MA (p17) (rabbit polyclonal, 1/200 dilution, NIH AIDS Reagent Program, Division of AIDS, NIH (Cat #4811) from Dr. Paul Spearman and Dr. Lingmei Ding). The secondary antibodies used were anti-Mouse IgG (H+L) Alexa Fluor 405 conjugate (goat polyclonal, 1/500 dilution, A-10011, Life Technologies), anti-Mouse IgG (H+L) Alexa Fluor 647 conjugate (donkey polyclonal, 1/500 dilution, A-31571, ThermoFisher scientific), anti-Rabbit IgG (H+L) Alexa Fluor 647 conjugate (donkey polyclonal, 1/500 dilution, A-31573, ThermoFisher scientific), anti-Mouse IgG (H+L) Alexa Fluor 647 conjugate (goat polyclonal, 1/500 till 1/500,000 dilution, 1.4 Alexa Fluor 647 molecules per antibody, 115-607-003, Dianova), anti-Mouse IgG (H+L) Alexa Fluor 633 conjugate (goat polyclonal, 1/500 dilution, A-21052, ThermoFisher scientific).

For particle permeabilization experiments, the viruses were mounted on poly-D-lysine coated slides as above and subjected to mild saponin treatment as described previously (35). Saponin is a surface-acting glycoside, with membrane permeabilizing properties (42). Therefore, it punctures small pores in the viral membrane. The particles were first washed with PBS and then treated with either PBS (no saponin condition) or 100 µg/ml saponin solution in PBS (saponin condition) for 5 min at room temperature. The samples were washed once with PBS, fixed with 4% PFA and stained as described above.

Accepted Manuscript Posted Online

Journal of Virology

JVI

Journal of Virology

Downloaded from http://jvi.asm.org/ on February 4, 2020 at 26989832

759 For estimating colocalization of fluorescent, particle-associated proteins in purified virions, the
760 immobilized particles were imaged in z-stacks of 6-12 0.3 um steps by confocal laser scanning
761 microscopy (CLSM). Emission from Alexa 405-stained p24, eGFP-tagged p24 and mCherry-labelled
762 integrase (IN) was detected after excitation with lasers of 405 nm, 488 nm and 559 nm, respectively.
763 Confocal microscopy was conducted with a 60 x apotome W NA=1.25.
764
765 **Capsid core purification**
766 Purification of intact HIV-1 cores was conducted as described previously (49). Briefly, fluorescent
767 virus particles were produced after transient transfection of 30 10 cm dishes of 293T cells (see
768 above). The supernatants were filtered, and virus was pelleted by ultracentrifugation (SW28 rotor,
769 133,000 x *g*, 2 h, 4 °C) through a 20% sucrose in PBS cushion. The pelleted viruses were resuspended
770 in a total of 1 ml of STE buffer (10 mM Tris-HCl pH 7.4, 100 mM NaCl, 1 mM EDTA) and then
771 subjected to core purification through layers of sucrose diluted in STE buffer. Continuous sucrose
772 gradients (10 ml, 30 – 70% sucrose) were mounted first into ultracentrifuge tubes, covered with 0.5
773 ml of 15% sucrose, followed by 0.5 ml of 10% sucrose and finally 0.5 ml virus suspension on top. The
774 virus was split into two equal parts. One half of the virus was loaded on the control gradient (no
775 detergent in the 15% sucrose layer), while the other virus half was loaded on a gradient with 15%
776 sucrose layer containing 1% Triton X-100.
777 The particles were spun through the gradients in an SW28 rotor, at 140,000 x *g* for 16 h over night at
778 4 °C. Afterwards, the tubes were placed on ice and 1 ml fractions were harvested into ice-cold
779 Eppendorf tubes. Fractions were analyzed for p24 content to determine the peak of core presence.
780 Core containing fractions were pooled together and snap frozen in liquid nitrogen until analysis.
781 Before analysis, core containing fractions were thawed on ice.
782
783 **Total internal reflection fluorescence (TIRF) microscopy**

Accepted Manuscript Posted Online

784 To determine the number of fluorescent molecules incorporated into single virus particles, wide-field
785 TIRF microscopy was performed. Quantification is possible after fluorescence intensity comparisons
786 between purified virus particles and a single molecule eGFP solution imaged under the same
787 conditions. Imaging was performed on an inverted microscope (Olympus IX-83, Olympus NV,
788 Aartselaar, Belgium) by objective-type total internal reflection excitation and wide-field detection.
789 Excitation was performed with 488-nm (Sapphire 488-100 CW, 100 mW, Coherent) and 644-nm laser
790 lines (Excelsior, Newport Spectra Physics BV, 100 mW). The laser lines were combined using
791 appropriate dichroic mirrors, the light was circularly polarised (WPQ05M-532, Thor-labs GmbH) and
792 expanded five times to achieve a homogenous beam profile, before being focused on the back focal
793 plane of the objective (PlanApo TIRF 60x, NA 1.45 oil, Olympus) through a 500-mm planoconvex
794 achromatic lens (KPX211-C BK7 Precision Plano-Convex lens, Newport). Emission light was collected
795 by the same objective and split by a polychromic mirror (z405/488/561/644rdc, Chroma) into two
796 separate channels for eGFP detection (a HQ590/40-2P emission filter) and p24 detection (LP655). The
797 fluorescence image was expanded 2.5-fold (PE eyepiece 125, 2.5x, Olympus) and focused onto the
798 electron multiplying charge coupled device EM-CCD (ImagEM, Hamamatsu Photonics, Louvain-La-
799 Neuve, Belgium). The image resolution was 512×512 pixels, with a pixel size of 107 nm. Movies were
800 recorded at 100 ms per frame with continuous acquisition. Intensity was determined using Localizer-
801 software (43).

802 **Acknowledgments**

803 We thank Paulien Van de Velde, Jooke Van der Veken and Barbara Van Remoortel for excellent
804 technical assistance. The following reagents were obtained through the NIH AIDS Research and
805 Reference Reagent Program, Division of AIDS, NIAID, NIH: pNL4-3.Luc.R–.E– plasmid (Cat #3418)
806 from Dr. Nathaniel Landau, mouse monoclonal anti-HIV-1 CA (p24) antibody (AG3.0) (Cat #4121)
807 from Dr. Jonathan Allan, raltegravir (Cat #11680) from Merck and Company, Inc. Research at KU
808 Leuven received financial support from the FWO, the KU Leuven Research Council (OT; OT/13/098

Downloaded from http://jvi.asm.org/ on February 4, 2020 at 26989832

Journal of Virology JVI Journal of Virology

Accepted Manuscript Posted Online

809 and C1 C14/17/095), HIV-ERA EURECA (IWT-SBO-EURECA, ZL345530), the KU Leuven IDO program
810 (IDO/12/008), the Belgian IAP Belvir (ZKC4893-P7/45-P).

811

812 **Author contributions**

813 I.Z.B., L.D., F.C., J. Hendrix, J. Hofkens and Z.D. conceived the study. I.Z.B., L.D., V.L., D.B. and F.D.W.
814 performed the experiments. I.Z.B., L.D., V.L., D.B., F.D.W., S.R., F.V., and Z.D. analyzed data. I.Z.B. and
815 Z.D. wrote the manuscript. All authors read and approved of the manuscript.

816

817 **Conflict of interest**

818 The authors declare that they have no conflict of interest.

819

820 **References**

821 1. Campbell EM, Hope TJ (2015) HIV-1 Capsid: The Multifaceted Key Player in HIV-1 infection. *Nat*
822 *Rev Microbiol* **13** (8): 471–483.
823 2. Ganser BK, Li S, Klishko VY, Finch JT, Sundquist WI (1999) Assembly and analysis of conical
824 models for the HIV-1 core. *Science* **283** (5398): 80-83
825 3. Li S, Hill CP, Sundquist WI, Finch JT (2000) Image reconstructions of helical assemblies of the
826 HIV-1 CA protein. *Nature* **407**: 409-413
827 4. Briggs JAG, Simon MN, Gross I, Kräusslich H-G, Fuller SD, Vogt VM, Johnson MC (2004) The
828 stoichiometry of Gag protein in HIV-1. *Nat Struct Mol Biol* **11**: 672-675
829 5. Yan N, Regalado-Magdos AD, Stiggelbout B, Lee-Kirsch MA, Lieberman J (2010) The cytosolic
830 exonuclease TREX1 inhibits the innate immune response to human immunodeficiency virus type
831 1. *Nat Immunol.* **11**: 1005-1013.
832 6. Rasaiyaah J, Tan CP, Fletcher AJ, Price AJ, Blondeau C, Hilditch L, Jacques DA, Selwood DL,
833 James LC, Noursadeghi M, Towers GJ (2013) HIV-1 evades innate immune recognition through
834 specific co-factor recruitment. *Nature* **503** (7476): 402–405.

Journal of Virology
JVI
Journal of Virology
Downloaded from http://jvi.asm.org/ on February 4, 2020 at 26989832

Accepted Manuscript Posted Online

7. Gao D, Wu J, Wu Y-T, Du F, Aroh C, Yan N, Sun L, Chen ZJ (2013) Cyclic GMP-AMP Synthase is an Innate Immune Sensor of HIV and Other Retroviruses. *Science* 10.1126/science.1240933.

8. Lahaye X, Satoh T, Gentili M, Cerboni S, Conrad C, Hurbain I, El Marjou A, Lacabaratz C, Lelièvre J-D, Manel N (2013) The capsids of HIV-1 and HIV-2 determine immune detection of the viral cDNA by the innate sensor cGAS in dendritic cells. *Immunity* **39** (6): 1132-1142

9. Forshey BM, von Schwedler U, Sundquist WI, Aiken C (2002) Formation of a Human Immunodeficiency Virus Type 1 Core of Optimal Stability Is Crucial for Viral Replication. *J Virol* **76** (11): 5667–5677.

10. Rankovic S, Varadarajan J, Ramalho R, Aiken C, Rousso I (2017) Reverse transcription mechanically initiates HIV-1 capsid disassembly. *J Virol* **91** (12): e00289-17

11. Mamede JI, Cianci GC, Anderson MR, Hope TJ (2017) Early cytoplasmic uncoating is associated with infectivity of HIV-1. *PNAS* **114** (34): E7169-78

12. Hübner W, Chen P, Portillo AD, Liu Y, Gordon RE, Chen BK (2007) Sequence of Human Immunodeficiency Virus Type 1 (HIV-1) Gag Localization and Oligomerization Monitored with Live Confocal Imaging of a Replication-Competent, Fluorescently Tagged HIV-1 . *J Virol* **81** (22): 12596–12607.

13. Padilla-Parra S, Marin M, Gahlaut N, Suter R, Kondo N, Melikyan GB (2013) Fusion of Mature HIV-1 Particles Leads to Complete Release of a Gag-GFP-Based Content Marker and Raises the Intraviral pH. *Plos One* **8** (8): e71002.

14. Hulme AE, Perez O, Hope TJ (2011) Complementary assays reveal a relationship between HIV-1 uncoating and reverse transcription. *PNAS* **108**:9975–9980.

15. Lukic Z, Dharan A, Fricke T, Diaz-Griffero F, Campbell EM (2014) HIV-1 Uncoating is Facilitated by Dynein and Kinesin-1. *J Virol* **88**: 13613–13625.

16. Perez-Caballero D, Hatziioannou T, Zhang F, Cowan S, Bieniasz PD (2005) Restriction of Human Immunodeficiency Virus Type 1 by TRIM-CypA Occurs with Rapid Kinetics and

Journal of Virology

JVI

Journal of Virology

Downloaded from http://jvi.asm.org/ on February 4, 2020 at 26989832

Accepted Manuscript Posted Online

Independently of Cytoplasmic Bodies, Ubiquitin, and Proteasome Activity. *J Virol* **79**: 15567–15572

17. Arhel NJ, Souquere-Besse S, Munier S, Souque P, Guadagnini S, Rutherford S, Prévost M-C, Allen TD, Charneau P (2007) HIV-1 DNA Flap formation promotes uncoating of the pre-integration complex at the nuclear pore. *EMBO J* **26** (12): 3025–3037.

18. Francis AC, Melikyan GB (2018) Single HIV-1 Imaging Reveals Progression of Infection through CA-Dependent Steps of Docking at the Nuclear Pore, Uncoating, and Nuclear Transport. *Cell Host Microbe* **23** (4):536-548

19. Miller MD, Farnet CM, Bushman FD (1997) Human immunodeficiency virus type 1 preintegration complexes: studies of organization and composition. *J Virol* **71** (7): 5382–5390.

20. Yamashita M, Emerman M (2004) Capsid Is a Dominant Determinant of Retrovirus Infectivity in Nondividing Cells. *J Virol* **78** (11): 5670–5678.

21. Yamashita M, Perez O, Hope TJ, Emerman M (2007) Evidence for Direct Involvement of the Capsid Protein in HIV Infection of Nondividing Cells. *Plos Pathog* **3** (10): e156

22. Price AJ, Jacques DA, McEwan WA, Fletcher AJ, Essig S, Chin JW, Halambage UD, Aiken C, James LC (2014) Host Cofactors and Pharmacologic Ligands Share an Essential Interface in HIV-1 Capsid That Is Lost upon Disassembly. *Plos Pathog* **10** (10): e1004459.

23. Peng K, Muranyi W, Glass B, Laketa V, Yant SR, Tsai L, Cihlar T, Müller B, Kraüsslich H-G (2014) Quantitative microscopy of functional HIV post-entry complexes reveals association of replication with the viral capsid. *ELife* **3**: e04114

24. Chin CR, Perreira JM, Savidis G, Portmann JM, Aker AM, Freeley EM, Smith MC, Brass AL (2015) Direct Visualization of HIV-1 Replication Intermediates shows that Viral Capsid and CPSF6 Modulate HIV-1 Intra-nuclear Invasion and Integration. *Cell Rep* **13** (8): 1717-31

25. Hulme AE, Kelley Z, Foley D, Hope TJ (2015) Complementary Assays Reveal a Low Level of CA Associated with Viral Complexes in the Nuclei of HIV-1-Infected Cells. *J Virol* **89** (10): 5350–5361.

Journal of Virology

JVI

Journal of Virology

Downloaded from http://jvi.asm.org/ on February 4, 2020 at 26989832

Accepted Manuscript Posted Online

885 26. Blair WS, Pickford C, Irving SL, Brown DG, Anderson M, Bazin R, Cao J, Ciaramella G, Isaacson
886 J, Jackson L, Hunt R, Kjerrstrom A, Nieman JA, Patick AK, Perros M, Scott AD, Whitby K, Hua W,
887 Butler SL (2010) HIV capsid is a tractable target for small molecule therapeutic intervention. *Plos*
888 *Pathog* **6**: e1001220
889 27. Shi J, Zhou J, Shah VB, Aiken C, Whitby K (2011) Small-Molecule Inhibition of Human
890 Immunodeficiency Virus Type 1 Infection by Virus Capsid Destabilization . *J Virol* **85** (1): 542–549.
891 28. Fricke T, Brandariz-Nuñez A, Wang X, Smith AB, Diaz-Griffero F (2013) Human Cytosolic
892 Extracts Stabilize the HIV-1 Core. *J Virol* **87** (19): 10587–10597.
893 29. Fricke T, Buffone C, Opp S, Valle-Casuso J, Diaz-Griffero F (2014) BI-2 destabilizes HIV-1 cores
894 during infection and Prevents Binding of CPSF6 to the HIV-1 Capsid. *Retrovirology* **11**: 120.
895 30. Zhou J, Price AJ, Halambage UD, James LC, Aiken C (2015) HIV-1 Resistance to the Capsid-
896 Targeting Inhibitor PF74 Results in Altered Dependence on Host Factors Required for Virus
897 Nuclear Entry. *J Virol* **89** (17): 9068–9079.
898 31. Chen B-C, Legant WR, Wang K, Shao L, Milkie DE, Davidson MW, Janetopoulos C, Wu XS,
899 Hammer JA, Liu Z, English BP, Mimori-Kiyosue Y, Romero DP, Ritter AT, Lippincott-Schwartz J,
900 Fritz-Laylin L, Mullins RD, Mitchell DM, Bembenek JN, Reymann AC, Böhme R, Grill SW, Wang JT,
901 Seydoux G, Tulu US, Kiehart DP, Betzig E (2014) Lattice light-sheet microscopy: Imaging molecules
902 to embryos at high spatiotemporal resolution. *Science* **346** (6208): 1257998
903 32. Albanese A, Arosio D, Terreni M, Cereseto A (2008) HIV-1 Pre-Integration Complexes
904 Selectively Target Decondensed Chromatin in the Nuclear Periphery. *Plos One* **3**, 2413.
905 33. Borrenberghs D, Dirix L, De Wit F, Rocha S, Blokken J, De Houwer S, Gijsbers R, Christ F,
906 Hofkens J, Hendrix J, Debyser Z (2016) Dynamic Oligomerization of Integrase Orchestrates HIV
907 Nuclear Entry. *Sci Rep* **6**: 36485.
908 34. Borrenberghs D, Thys W, Rocha S, Demeulemeester J, Weydert C, Dedecker P, Hofkens J,
909 Debyser Z, Hendrix J (2014) HIV virions as nanoscopic test tubes for probing oligomerization of
910 the integrase enzyme. *ACS Nano* **8** (4): 3531-45

Downloaded from http://jvi.asm.org/ on February 4, 2020 at 26989832

Journal of Virology JVI Journal of Virology

Accepted Manuscript Posted Online

911 35. Francis AC, Marin M, Shi J, Aiken C, Melikyan GB (2016) Time resolved imaging of single HIV1
912 uncoating in vitro and in living cells. *Plos Pathog* **12** (6): e1005709
913 36. Matreyek KA, Yücel SS, Engelman A (2013) Nucleoporin NUP153 Phenylalanine-Glycine Motifs
914 Engage a Common binding pocket within the HIV-1 Capsid Protein to Mediate Lentiviral
915 Infectivity. *Plos Pathog* **9** (10): e1003693
916 37. Campbell EM, Perez O, Anderson JL, Hope TJ (2008) Visualization of a proteasome-
917 independent intermediate during restriction of HIV-1 by rhesus TRIM5α. *JCB* **180** (3): 549–561.
918 38. Pereira CF, Ellenberg PC, Jones KL, Fernandez TL, Smyth RP, Hawkes DJ, Hijnen M, Vivet-
919 Boudou V, Marquet R, Johnson I, Mak J (2011) Labelling of multiple HIV-1 proteins with the
920 biarsenical tetracysteine system. *Plos One* **6** (2): e17016.
921 39. He J, Choe S, Walker R, Di Marzio P, Morgan DO, Landau NR (1995) Human immunodeficiency
922 virus type 1 viral protein R (Vpr) arrests cells in the G2 phase of the cell cycle by inhibiting
923 p34cdc2 activity. *J Virol* **69**: 6705-6711.
924 40. Pizzato M, Erlwein O, Bonsall D, Kaye S, Muir D, McClure MO (2009) A one-step SYBR Green I-
925 based product-enhanced reverse transcriptase assay for the quantitation of retroviruses in cell
926 culture supernatants. *J Virol Methods* **156** (1-2): 1-7
927 41. Vermeire J, Naessens E, Vanderstraeten H, Landi A, Iannucci V, Van Nuffel A, Taghon T,
928 Pizzato M, Verhasselt B (2012) Quantification of Reverse Transcriptase Activity by Real-Time PCR
929 as a Fast and Accurate Method for Titration of HIV, Lenti- and Retroviral Vectors. *Plos One* **7** (12):
930 e50859.
931 42. Francis G, Kerem Z, Makkar HP, Becker K (2002) The biological action of saponins in animal
932 systems: a review. *Br J Nutr* **88**: 587–605.
933 43. Dedecker P, Duwe S, Neely RK, Zhang J (2012) Localizer: fast, accurate, open-source, and
934 modular software package for superresolution microscopy. *J Biomed Opt* **17**(12):126008.
935 44. Zack GW, Rogers WE, Latt SA (1977) Automatic measurement of sister chromatid exchange
936 frequency. *J Histochem Cytochem* **25**: 741–753

Downloaded from http://jvi.asm.org/ on February 4, 2020 at 26989832

Journal of Virology
JVI
Journal of Virology

Accepted Manuscript Posted Online

937 45. Ambrose Z, Aiken C (2014) HIV-1 Uncoating: Connection to Nuclear Entry and Regulation by
938 Host Proteins. *Virology* **0**: 371–379.

939 46. Bhattacharya A, Alam SL, Fricke T, Zadrozny K, Sedzicki J, Taylor AB, Demeler B, Pornillos O,
940 Ganser-Pornillos BK, Diaz-Griffero F, Ivanov DN, Yeager M (2014) Structural basis of HIV-1 capsid
941 recognition by PF74 and CPSF6. PNAS **111** (52): 18625–18630.

942 47. Briggs JAG, Wilk T, Welker R, Kräusslich H-G, Fuller SD (2003) Structural organization of
943 authentic, mature HIV-1 virions and cores. *EMBO J* **22** (7): 1707-1715.

944 48. McDonald D, Vodicka MA, Lucero G, Svitkina TM, Borisy GG, Emerman M, Hope TJ (2002)
945 Visualization of the intracellular behavior of HIV in living cells. *JCB* **159** (3): 441–452.

946 49. Shah VB, Aiken C (2011). In vitro Uncoating of HIV-1 Cores. *J Vis Exp* (57), 3384.

947 50. Sowd GA, Serrao E, Wang H, Wang W, Fadel HJ, Poeschla EM, Engelman AN (2016) A critical
948 role for alternative polyadenylation factor CPSF6 in targeting HIV-1 integration to
949 transcriptionally active chromatin. *PNAS* **113** (8): E1054–E1063

950 51. Achuthan V, Pereira JM, Sowd GA, Puray-Chavez M, McDougall WM, Paulucci-Holthauzen A,
951 Wu X, Fadel HJ, Poeschla EM, Multani AS, Hughes SH, Sarafianos SG, Brass AL, Engelman AN
952 (2018) Capsid-CPSF6 interaction licenses HIV-1 nuclear trafficking to sites of viral DNA
953 integration. *Cell Host Microbe* **24** (3): 392-404

954 52. Martin BR, Giepmans BNG, Adams SR, Tsien RY (2005) Mammalian cell-based optimization of
955 the biarsenical-binding tetracysteine motif for improved fluorescence and affinity. *Nat Biotech*
956 **23**: 1308-1314

957 53. Chiu J, March PE, Lee R, Tillett D (2004) Site-directed, Ligase-Independent Mutagenesis
958 (SLIM): a single-tube methodology approaching 100% efficiency in 4 h. *Nucleic Acids Res* **32**
959 (21):e174. doi:10.1093/nar/gnh172

960 54. Márquez CL, Lau D, Walsh J, Shah V, McGuinness C, Wong A, Aggarwal A, Parker MW, Jacques
961 DA, Turville S, Böcking T (2018) Kinetics of HIV-1 capsid uncoating revealed by single-molecule
962 analysis. *Elife* **7**:e34772. doi:10.7554/eLife.34772

Journal of Virology
JVI
Journal of Virology
Downloaded from http://jvi.asm.org/ on February 4, 2020 at 26989832

Accepted Manuscript Posted Online

963 55. Schaller T, Ocwieja KE, Rasaiyaah J, Price AJ, Brady TL, Roth SL, Hué S, Fletcher AJ, Lee K,
964 KewalRamani VN, Noursadeghi M, Jenner RG, James LC, Bushman FD, Towers GJ (2011) HIV-1
965 capsid-cyclophilin interactions determine nuclear import pathway, integration targeting and
966 replication efficiency. *PLoS Pathog*. **7**(12):e1002439. doi:10.1371/journal.ppat.1002439
967 56. Lee K, Ambrose Z, Martin TD, Oztop I, Mulky A, Julias JG, Vandegraaff N, Baumann JG, Wang J,
968 Yuen W, Takemura T, Shelton K, Taniuchi I, Li Y, Sodroski J, Littman DR, Coffin JM, Hughes SH,
969 Unutmaz D, Engelman A, KewalRamani VN (2010) Flexible use of nuclear import pathways by
970 HIV-1. *Cell Host Microbe*. **7**(3):221–233. doi:10.1016/j.chom.2010.02.007
971 57. Rasheedi S, Shun MC, Serrao E, Sowd GA, Qian J, Hao C, Dasgupta T, Engelman AN,
972 Skowronski J (2016) The Cleavage and Polyadenylation Specificity Factor 6 (CPSF6) Subunit of the
973 Capsid-recruited Pre-messenger RNA Cleavage Factor I (CFIm) Complex Mediates HIV-1
974 Integration into Genes. *J Biol Chem*. **291**(22):11809–11819. doi:10.1074/jbc.M116.721647
975 58. Borrenberghs D, Zurnic I, De Wit F, Acke A, Dirix L, Cereseto A, Debyser Z, Hendrix J (2018)
976 Post-mitotic BET-induced reshaping of integrase quaternary structure supports wild-type MLV
977 integration *Nucleic Acids Res*. **47**(3):1195–1210. doi:10.1093/nar/gky1157
978 59. Stirnnagel K, Lüftenegger D, Stange A, Swiersy A, Müllers E, Reh J, Stanke N, Große A, Chiantia
979 S, Keller H, Schwille P, Hanenberg H, Zentgraf H, Lindemann D (2010) Analysis of prototype foamy
980 virus particle-host cell interaction with autofluorescent retroviral particles. *Retrovirology*. **7**:45.
981 doi:10.1186/1742-4690-7-45
982 60. Verkhusha VV and Sorkin A (2005) Conversion of the monomeric red fluorescent protein into
983 a photoactivatable probe. Chem Biol. **12**:279–285. doi: 10.1016/j.chembiol.2005.01.005.
984 61. Vansant G, Vranckx LS, Zurnic I, Van Looveren D, Van de Velde P, Nobles C, Gijsbers R, Christ
985 F, Debyser Z (2019) Impact of LEDGIN treatment during virus production on residual HIV-1
986 transcription. *Retrovirology*. **16**(1):8. doi:10.1186/s12977-019-0472-3

Journal of Virology
JVI
Journal of Virology
Downloaded from http://jvi.asm.org/ on February 4, 2020 at 26989832

Accepted Manuscript Posted Online

62. Thys W, De Houwer S, Demeulemeester J, Taltynov O, Vancraenenbroeck R, Gérard M, De Rijck J, Gijsbers R, Christ F, Debyser Z (2011) Interplay between HIV entry and transportin-SR2 dependency. *Retrovirology*. **8**:7. doi:10.1186/1742-4690-8-7

Figure legends:

Figure 1: Schematic representation of CA tagging strategies. A. Amino acid sequence and primary structure of HIV-1 CA, with tC motif insertions highlighted in light green below the sequence. Important alpha helices and domains are marked in dark green on the level of the sequence. H1-H11: alpha helices number 1 to 11; CypA: cyclophylin A binding motif. B1: beta sheet 1; **B.** Secondary structure of a CA monomer, as found in the CA hexamer (PDB: 3H4E), with tC insertions highlighted in light green, corresponding to the A panel Orange: N-terminal domain (NTD); Blue: C-terminal domain (CTD). **C.** Schematic representation of tC or eGFP tag fusions to the CA N- or C-terminus, respectively. Reintroduced protease cleavage sites are indicated in dark red and linkers for optimal eGFP folding are indicated in light green. tC tags are highlighted in orange. **D.** Recombinant, VSV-G pseudotyped virus particles were produced by transfection as outlined in Material and Methods. For transfections, different ratios of the pNL4-3.Luc.R-E- derivatives (coding for either the tC- or the eGFP-tagged CA) and the original pNL4-3.Luc.R-E construct were mixed as indicated in the x-axes (0:1, 1:0, 1:2 and 1:10). The positions of tC and eGFP tags in each virus prep are indicated above corresponding plots. Virus particles were harvested and filtered, and particle release was assessed by p24 ELISA and SG-PERT (indicated RT in the graph). Particle release values of viruses carrying only the original pNL4-3.Luc.R-E- construct (0:1) were arbitrarily set to 100% and error bars represent standard deviations of triplicates. Data are derived from one representative out of n=2 independent experiments.

Figure 2: Transduction efficiency of single- and dually-labelled viruses (accompanying Figure 1). Recombinant, VSV-G pseudotyped virus particles were produced by transfection as outlined in Material and Methods. For transfections, different ratios of the pNL4-3.Luc.R-E- derivatives (coding

Journal of Virology
JVI
Journal of Virology
Downloaded from http://jvi.asm.org/ on February 4, 2020 at 26989832

Accepted Manuscript Posted Online

Journal of Virology

JVI

Journal of Virology

Downloaded from http://jvi.asm.org/ on February 4, 2020 at 26989832

1013 for either the tC- or the eGFP-tagged CA) and the original pNL4-3.Luc.R-E construct were mixed as
1014 indicated in the x-axes (0:1, 1:0, 1:2 and 1:10). The positions of tC and eGFP tags in each virus prep
1015 are indicated above the corresponding plots. Virus particles were harvested and filtered, and particle
1016 release was assessed by p24 ELISA. Transduction efficiencies of these particles were evaluated three
1017 days post transduction of HeLa P4 cells and are represented as RLU values of the fLuc reporter
1018 readout. Error bars represent standard deviations of triplicates. Data are derived from one
1019 representative out of n=2 independent experiments.
1020
1021 **Figure 3: IN-mCherry labelling yields particles comparable with IN-eGFP containing virions.**
1022 Replication-deficient virus particles were produced by transiently transfecting 293T cells with pNL4-
1023 3.Luc. R-E-, pVpr-IN-FP (IN-mCherry or IN-eGFP, indicated on the x-axes) and pVSV-G constructs. **A.**
1024 Virus particle release was quantified by p24 ELISA and SG-PERT (RT activity) of purified particles and
1025 expressed relative to one another. The yields of IN-mCherry containing viruses were arbitrarily set to
1026 100%. The data represent mean ± standard deviation (SD) of triplicates. **B.** HeLaP4 cells were
1027 transduced with normalized amounts of fluorescent viruses and firefly luciferase (fLuc) reporter
1028 levels were assayed three days post transduction. Luciferase readout was normalized to the total
1029 protein input (determined by BCA assay) and expressed as relative light units (RLU). Data are mean ±
1030 SD of triplicates. **C.** Representative images of purified viruses containing IN labels (IN-eGFP and IN-
1031 mCherry). Particles were adhered to microscopic slides for 4 h at 37 °C and were then fixed with PFA
1032 and immunostained using AG3.0 p24 antibody. The channels in which p24 staining (blue) or IN-FP
1033 fluorescence (magenta) were detected are indicated in corresponding pseudocolors. For each type of
1034 particles, the merged image is shown at the end of each panel as the overlay of two pseudocolors.
1035 The overall image brightness was improved in ImageJ software for clarity purposes. Scale bar: 5 µm.
1036 **D-F.** HeLaP4 cells were transduced with IN-FP labelled viruses, fixed 6h post infection and nuclear
1037 envelope was defined by lamin A/C immunostaining. The cells were imaged by confocal microscopy
1038 and numbers and fluorescence intensities of IN-FP complexes were determined in each subcellular

Accepted Manuscript Posted Online

Journal of Virology

JVI

Journal of Virology

Downloaded from http://jvi.asm.org/ on February 4, 2020 at 26989832

compartment (cytoplasm, nuclear envelope, nucleus; consult Figure 7A for clarification). Data are derived from n=1 experiment. **D.** The number of IN-FP complexes per cell is represented by box and whisker plots for each virus. **E.** Percentage of nuclear IN-FP complexes per condition. The percentage was calculated as the fraction of IN-FP complexes localized in infected cell nuclei compared to the total number of IN-FP complexes detected in the experiment. Error bars represent SD values. **F.** IN-FP complex intensities were measured as previously described (33) and plotted for each compartment (cytoplasm, nuclear envelope, nucleus). The bars represent the mean ± SD values. As indicated elsewhere, the intensities significantly differ between the cytoplasm and the nucleus ($p<0.001$, two-tailed t-test with equal variance assumed).

Figure 4: Schematic outline of the experimental setup and optimization of fluorescent CA labelling. **A**. Constructs used for fluorescent labelling of replication-deficient, VSV-G pseudotyped virus particles. The eGFP tag was fused to the C-terminus of capsid via the DPPVAT linker, in the context of the pNL4-3.Luc.R-E- transfer and packaging construct. mCherry was fused to the integrase C-terminus by replacement of the eGFP open reading frame (ORF) with the mCherry ORF in the context of the pVpr-IN-FP construct (32, 33, 34). Labelled virus particles were produced by transient transfection of pLP-VSV-G, pVpr-IN-mCherry, pNL4-3.Luc. R-E- and (only for double-labelled viruses) pNL4-3.Luc. R-E-CA-eGFP into 293T cells. Virus supernatants were harvested and concentrated as described in Material and Methods. Dashed lines indicate viral protease cleavage sites. *Δenv* and *Δnef* indicate *env* and *nef* shortened open reading frames, respectively. **B**. Unlabelled particles (WT), particles with IN-mCh (WT-mCh) and double-labelled particles (CA-eGFP) containing also the labelled capsid (using pNL4-3.Luc. R-E- CA-eGFP and WT pNL4-3.Luc.R-E- constructs in a ratio 1:2 or 1:10) were produced as described above. Endogenous reverse transcriptase activity was assessed by SG-PERT. Values are derived from one experiment. Data are presented normalized to the unlabelled (WT) virus levels. **C**. Single-round transduction efficiencies of unlabelled and labelled virions. Unlabelled, single- and double-labelled viruses were produced and concentrated as described in Material and Methods. Unlabelled particles (WT) were produced by transfection of the parental luciferase-coding vector in

Accepted Manuscript Posted Online

Journal of Virology

JVI

Journal of Virology

Downloaded from http://jvi.asm.org/ on February 4, 2020 at 26989832

combination with the VSV-G-coding plasmid. Single-labelled particles contained IN-mCherry after addition of Vpr-INmCh to the parental luciferase construct. Double-labelled particles all contained IN-mCherry and CA-eGFP produced with a CA-eGFP to WT pNL4-3.Luc.R-E- vector ratio of 1:2 or 1:10, respectively). Single-round transduction efficiency was determined by firefly luciferase (fLuc) levels in HeLaP4 cells transduced with serial dilutions of virus supernatants (starting amounts were normalized for endogenous RT activity and virus dilutions are shown on the x-axis). Relative light units (RLU) were measured three days post transduction and represent a relative value obtained after normalizing the fLuc signal for protein content using the BCA assay. Data are derived from one experiment.

Figure 5: CA-eGFP is incorporated into extracellular HIV-1 virions. Virions containing only the IN-mCherry label are marked as WT-mCh, while double-labelled virions (containing CA-eGFP in addition to IN-mCherry) are always indicated as CA-eGFP, with the ratio of labelled to unlabelled capsid (pNL4-3.Luc. R-E- CA-eGFP to WT pNL4-3.Luc.R-E-) 1:10 in the annotation. Data are derived from one representative out of n≥3 experiments. **A**. Virus particles were allowed to attach to microscopic slides for 4 h at 37 °C and were then fixed and immunostained with AG3.0 p24-specific antibody, followed by secondary antibody conjugated to Alexa 405. Fluorescent signals originating from p24 staining (blue), IN-mCherry (not shown; see Figure 3C) and CA-eGFP (green) are shown in corresponding pseudocolors. Overlay of the channels showing p24 staining and CA-eGFP signals is shown under 'merge' panels. Upper panel: particles containing only IN-mCherry (single-labelled viruses). Lower panel: particles containing both IN-mCherry and CA-eGFP labels, where ratio of labelled to unlabelled pNL4-3.Luc.R-E- vector was 1:10. Particles only stained by p24 are indicated by blue arrows, while those in which the CA-eGFP label colocalizes with p24 staining are indicated by white arrows. The overall image brightness was improved in ImageJ software for clarity purposes. Scale bar: 5 µm. **B.** CA-eGFP labelling efficiency was determined as the percent of all p24 stained particles that also contained CA-eGFP. The labelling efficiency is shown for both CA-eGFP 1:2 and CA-eGFP 1:10 particles, where the values are plotted as the mean ± standard deviation. Data are derived

Accepted Manuscript Posted Online

Journal of Virology

JVI

Journal of Virology

Downloaded from http://jvi.asm.org/ on February 4, 2020 at 26989832

1091 from n≥3 independent experiments. **C**. The number of CA-eGFP molecules per particle was
1092 determined in comparison with a monomeric eGFP solution, both of which were imaged by wide-
1093 field TIRF microscopy as in Material and Methods. The ratio between fluorescence intensity of the
1094 spotted particles to monomeric eGFP was used to estimate CA-eGFP incorporation into single virions.
1095 **D**. Recombinant virus particles and 293T producer cells were lysed with 1% SDS and proteins were
1096 separated on a gradient gel (4-15%) SDS-PAGE. HIV capsid (CA; p24) and eGFP were detected with
1097 the corresponding antibodies, annotated below each figure panel. A molecular weight ladder is
1098 present next to each membrane and expected protein sizes are indicated by arrowheads. As in panel
1099 A, single- and dual particle labelling is indicated at the top of each panel (WT-mCh or CA-eGFP). For
1100 producer cell lysates, the marking indicates constructs used for transfection (in addition to the pLP-
1101 VSV-G and NL4-3 based transfer vector): WT-mCh indicates only Vpr-IN-mCherry was transfected,
1102 while CA-eGFP 1:2, 1:5 and 1:10 indicates additional cotransfection of the CA-eGFP coding transfer
1103 vector at the respective ratios. One representative experiment is shown for n=2 experiments.
1104 **Figure 6: eGFP-tagged capsid is associated with the viral core**. **A**. Schematic outline of saponin-
1105 mediated particle permeabilization (adapted from 35). Saponin punctures small pores in the viral
1106 membrane, causing all content not stably incorporated in the capsid core or embedded inside the
1107 core to dissociate. Upon washing, only the core-associated content remains. **B.** Recombinant virus
1108 particles were produced to contain IN-mCherry and CA-eGFP and mounted on poly-D-lysine coated
1109 microscopic slides (see Methods). The particles were treated for 5 min with either PBS or 100 µg/ml
1110 saponin, washed, fixed in 4% PFA and immunostained with p24 specific antibody (AG3.0). IN-mCherry
1111 (not shown), CA-eGFP or p24-Alexa 405 fluorescence were detected in corresponding fluorescence
1112 channels and particles were identified by in-house Matlab routines. Merged images were produced
1113 to show overlap of all three channels. White arrows indicate overlap of the three fluorophores,
1114 indicating intact capsid cores. Scale bar: 5 µm. **C.** Fluorescence intensities of CA-eGFP in PBS or
1115 saponin-treated virus particles. Viruses were analyzed by an in-house Matlab routine, as described in
1116 Materials and Methods. Intensities are plotted in 5-95% box-and-whisker plots. Data are derived

Accepted Manuscript Posted Online

Journal of Virology

JVI

Journal of Virology

Downloaded from http://jvi.asm.org/ on February 4, 2020 at 26989832

1117 from one representative out of n=3 independent experiments. **D.** Schematic outline of HIV-1 capsid
1118 core purification (as described in 49). Recombinant virus particles were produced as described (see
1119 Materials and Methods) and pelleted by ultracentrifugation through a 20% sucrose cushion. The
1120 particles were resuspended in cold STE buffer and loaded atop several layers with increasing
1121 concentrations of sucrose dissolved in STE buffer. In the presence of Triton in the 15% sucrose layer,
1122 the virus membrane is stripped off the particles during centrifugation. The cores remain intact and
1123 accumulate in the lowest fractions during centrifugation. In the absence of Triton, virus particles
1124 remain intact and accumulate in the middle gradient fractions, due to their lower density compared
1125 to the viral cores (1.18 g/ml density in comparison to 1.24 g/ml density of cores). **E**. Viral cores were
1126 purified by ultracentrifugation of concentrated particles through the detergent layer and continuous
1127 sucrose cushion and fractions containing viral cores were collected and combined. The core
1128 suspension was attached to microscopic slides for 20 min at room temperature, after which the
1129 samples were fixed and immunostained with the p24-specific antibody (mouse AG3.0). The cores
1130 were imaged under the confocal microscope and identified by in-house Matlab routines. White
1131 arrowheads denote complexes containing CA-eGFP, which also stain positive for p24. The overall
1132 image brightness was improved in ImageJ software for clarity purposes. Scale bar: 5 µm.

1133 **Figure 7: IN-mCherry and CA-eGFP complexes display distinct subcellular distributions early on**
1134 **after infection.** Recombinant and fluorescently labelled viruses were produced as outlined in Figure
1135 4A. WT-mCh particles contain only the IN-mCherry protein and their cell entry features were
1136 compared to double-labelled viruses, containing CA-eGFP at different ratios to unlabelled capsid (1:2
1137 and 1:10, as annotated in the graphs). **A**. Workflow of a single-virus imaging experiment. HeLaP4 cells
1138 were transduced with single- or double-labelled viruses, fixed and immunostained with a nuclear
1139 lamina specific antibody. The stained nuclear lamina is used as a reference to localize fluorescent
1140 viral complexes to either the cytoplasm (i), the nuclear envelope (ii) or the nucleus (iii). Cells were
1141 imaged by laser scanning confocal microscopy in Z-stacks. The image on the right shows a
1142 representative Z-stack of a HeLaP4 cell transduced with IN-mCherry and CA-eGFP labelled virions 6 h

Accepted Manuscript Posted Online

Journal of Virology

JVI

Journal of Virology

Downloaded from http://jvi.asm.org/ on February 4, 2020 at 26989832

1143 post transduction. The nuclear envelope is indicated by lamin staining (blue) and IN-mCherry and CA-
1144 eGFP containing viral complexes are depicted in magenta and green, respectively. White arrows
1145 indicate double-labelled fluorescent viral complexes. Scale bar: 10 µM. For each experiment, cells are
1146 imaged in Z-stacks, with a 0.3 µm step size and viral complexes are identified by an in-house Matlab
1147 routine as described previously (33). Each fluorescent viral complex was automatically detected and
1148 localized using in-house Matlab routines. **B-I.** HeLaP4 cells were transduced with recombinant
1149 particles and fluorescent complexes were identified and characterized in these cells 6 h after
1150 transduction, using in-house Matlab routines. Based on nuclear lamina staining, viral PICs were
1151 assigned to one of the three intracellular compartments (cytoplasm, nuclear envelope, nucleus).
1152 Numbers (**B, D, G**) and fluorescence intensities (**C** and **E**) of viral complexes were measured for each
1153 complex and are shown for IN-mCherry (**B** and **C**) and CA-eGFP (**D** and **E**). Shown are the data from
1154 one representative out of n=2 experiments. The complex numbers and intensities are plotted into 5-
1155 95% box and whisker plots, where the line in the box represents the median number and whiskers
1156 represent outliers. **B.** Intracellular distributions of IN-mCherry labelled complexes after transduction
1157 of HeLaP4 cells with single- (WT-mCh) or double-labelled (CA-eGFP 1:2 and CA-eGFP 1:10) virions.
1158 Percentage of nuclear IN-mCherry complexes, as an indicator of nuclear import, was calculated per
1159 cell and is indicated at the top of the graph, where each value represents percentage mean ± SEM.
1160 Statistical significance was determined by the Mann-Whitney test. * $p<0.05$; n.s. not significant. **C**.
1161 Fluorescence intensities of IN-mCherry complexes in each subcellular compartment (cytosol, nuclear
1162 envelope, nucleus). **D**. Intracellular distributions of CA-eGFP labelled complexes after transduction of
1163 HeLaP4 cells with single- (WT-mCh) or double-labelled (CA-eGFP 1:2 and CA-eGFP 1:10) virions. **E**.
1164 Fluorescence intensities of CA-eGFP complexes in transduced cells, shown for each subcellular
1165 compartment (cytosol, nuclear envelope, nucleus). **F**. Percentage of CA-eGFP complexes (relative to
1166 total intracellular CA-eGFP complex numbers) with high eGFP fluorescence intensity. **G**. Intracellular
1167 distribution of IN-mCherry + CA-eGFP labelled complexes upon transduction of HeLaP4 cells with
1168 single- (WT-mCh) or double-labelled (CA-eGFP 1:2 and CA-eGFP 1:10) virions. **H.** and **I.** Fractions of

Accepted Manuscript Posted Online

IN-mCherry (**H**) or CA-eGFP (**I**) complexes that belong to the colocalizing complexes (containing both fluorophores) were calculated as the number of colocalizing complexes divided by the number of total IN-mCherry or CA-eGFP PICs per cell. Values are expressed as mean ± SD.

Figure 8: Fluorescent viral complexes are derived from fusion-competent virus particles. Recombinant virus particles or virus-like particles (VLPs) were produced by transient transfection of the HIV-1 pNL4-3.Luc.R-E- vector and pVpr-IN-mCherry, as described in Methods, with or without the VSV-G encoding construct, respectively. Same virus particle and VLP amounts (as determined by p24 ELISA) were used to synchronously transduce HeLaP4 cells, which were fixed and immunostained with nuclear lamin antibodies at 1.5 h (**A**) or 6 h (**B**) post transduction. Viruses containing IN-mCherry (WT-mCh) or IN-mCherry and CA-eGFP (CA-eGFP 1:10) are annotated according to their label, whereas the corresponding VLPs are indicated as VLP next to the label name. The numbers of IN-mCherry or CA-eGFP complexes per cell are plotted in 5-95% box and whisker plots, where the line inside the box represents the median and whiskers represent the outliers. Groups were compared within the same intracellular compartment (e.g. cytosol WT-mCh VLP versus cytosol WT-mCh) and statistical significance was determined by the Mann-Whitney test. Significance is represented by * $p<0.05$, ** $p<0.005$ and *** $p<0.001$. Lack of annotation represents no statistical significance found between groups. Data are derived from one out of $n\geq2$ independent experiments.

Figure 9: PF74 inhibits nuclear import of IN-mCherry and CA-eGFP complexes. HeLaP4 cells were infected with single- (WT-mCh) or double (1:10)-labelled virions in the presence of DMSO or increasing PF74 concentrations (2 µM or 10 µM) and fixed at 1.5 h or 6 h post infection. Viral complexes were localized and fitted to a 2D Gaussian distribution by the published in-house Matlab routines. **A**. Representative images of transduced HeLaP4 cells fixed 6 h post infection. Nuclear lamina (defined as shown in Figure 4B) and viral complexes are indicated in corresponding colors (lamina, white; IN-mCherry, magenta and CA-eGFP, green). Complexes containing only IN-mCherry or CA-eGFP are indicated by magenta and green arrows, respectively. Complexes containing both fluorophores are indicated by white arrows. Scale bar: 10 µm. **B-E:** Data are grouped according to the

Journal of Virology JVI Journal of Virology

Downloaded from http://jvi.asm.org/ on February 4, 2020 at 26989832

Accepted Manuscript Posted Online

virus used (WT-mCh - single, IN-mCherry labelled particles; CA-eGFP 1:10 or 1:10 - double, IN-mCherry + CA-eGFP labelled virus particles) and to the intracellular compartment (cytoplasm, nuclear envelope and nucleus) in which the complexes were found. Data are presented in box-whisker plots, with the whiskers representing standard deviation, the box representing the mean value and the line representing the median. Data represent averages of n=2 independent experiments. Statistically significant differences in PIC numbers were analyzed by the Mann-Whitney test and indicate * $p<0.05$ and *** $p<0.001$. Lack of significance annotation indicates no statistical difference between the samples. **B** and **D**. Numbers of intracellular IN-mCherry containing complexes at 1.5 h (**B**) and 6 h (**D**) post infection. **C** and **E**. Numbers of intracellular CA-eGFP containing complexes at 1.5 h (**C**) and 6 h (**E**) post infection.

Figure 10: Fluorescent complex intensities under DMSO or PF74 treatment at 1.5 h or 6 h post transduction. HeLaP4 cells were transduced with IN-mCherry (WT-mCh) or IN-mCherry + CA-eGFP (CA-eGFP 1:10) labelled viruses and fixed at 1.5 h or 6 h post transduction. Transduction was performed in the presence of DMSO or two different PF74 concentrations (2 µM or 10 µM). Viral complexes were identified and characterized using in-house Matlab routines. Integrated fluorescence intensities of single viral complexes were plotted in 5-95% box and whisker plots (with features as described) and are shown for 1.5 h (**A, B**) or 6 h (**C, D**) post infection. Data are averages of n=2 independent experiments. Statistical analysis of intensity differences was done by the Kruskal-Wallis test with unequal variance and is indicated as * $p<0.05$, ** $p<0.01$ and *** $p<0.0001$. The lack of significance annotation indicates no statistical significance. **E.** Comparison of IN-mCherry and CA-eGFP intensities in intact particles versus intracellular virus complexes. Double-labelled viruses were produced as in Materials and Methods. The particles were spotted on microscopic glass coverslips, fixed and immunostained with the p24 antibody to detect single virus particles. The same virus prep was used in parallel to infect HeLa P4 cells. Fixed viruses and infected cells were imaged in the same experiment and under the same conditions. Fluorescent complexes were identified and characterized using an in-house Matlab routine. The spotted viruses are denoted as “particles” and intracellular

Journal of Virology JVI Journal of Virology

Downloaded from http://jvi.asm.org/ on February 4, 2020 at 26989832

Accepted Manuscript Posted Online

Journal of Virology

JVI

Journal of Virology

Downloaded from http://jvi.asm.org/ on February 4, 2020 at 26989832

virus complexes are denoted according to the compartment (cytoplasm, nuclear envelope, nucleus). Fluorescence intensities of viral complexes were measured for each complex and are shown for both CA-eGFP and IN-mCherry. The complex intensities are plotted into 5-95% box and whisker plots, where the line in the box represents the median number and the whiskers represent outliers. **F.** Median intensities ± standard deviation for all identified complexes are shown in the table. Shown are the data from one representative out of n=2 experiments.

Figure 11: Transduction efficiency and quantification of viral DNA upon transduction of HeLa P4 cells with unlabelled, single- and dually-labelled viruses (Supplementary to Figures 3 and 6). Recombinant VSV-G-pseudotyped viruses were produced and concentrated as described in Materials and Methods. For production of unlabelled particles (WT), only the parental pNL4-3.Luc.R-E- vector was used in combination with the pLP-VSV-G plasmid. Single- (WT-mCh) and dually-labelled particles were produced as described above, with two different ratios (1:2 and 1:10) CA-eGFP coding vector to the parental pNL4-3.Luc.R-E- plasmid in the case of dually-labelled virions (ratios indicated in figure legend). **A.** HeLa P4 cells were seeded for transduction as described in Materials and Methods. The following day, the cells were pre-treated with DMSO, 2 µM or 10 µM PF74 prior to transduction with different dilutions of virus (indicated on the x-axes). All transductions were done in parallel in the same experiment, using virus supernatants produced in parallel. The virus dilutions were made starting from RT-normalized supernatants. Transduction efficiencies were determined by fLuc activity, normalized for total protein content (BCA). Data are plotted as the mean ± SD of biological triplicates. **B.** Quantification of total viral DNA in transduced HeLa cells seven days post transduction. Genomic DNA was extracted from transduced cells and viral DNA was quantified by means of Gag-specific qpCR. Viral DNA copies were normalized for cellular input via the CCR5-specific qPCR. Viral DNA levels in cells transduced with unlabelled (WT) virus were arbitrarily set to 100% and all other transduced samples (labelled according to the virus used) were plotted relative to the WT. Data are plotted as the mean ± SD of biological duplicates.

Accepted Manuscript Posted Online

Journal of Virology

JVI

Journal of Virology

Downloaded from http://jvi.asm.org/ on February 4, 2020 at 26989832

Figure 12: Impact of integrase inhibition on CA-eGFP and IN-mCherry complexes in the nucleus. HeLaP4 cells were transduced with IN-mCherry (WT-mCh) or IN-mCherry+CA-eGFP (CA-eGFP 1:10) viruses in the presence of DMSO or 0.6 µM RAL. Cells were fixed at 6 h post transduction, the nuclear lamina was immunostained and viral IN-mCherry and CA-eGFP complexes were identified and localized using the described, in-house Matlab routines (see Methods). Percentage of IN-mCherry (**A**), CA-eGFP (**B**) and double labelled complexes (CA-eGFP+IN-mCherry) (**C** and **D**) was determined out of the total complex number per cell and values are plotted as mean ± SEM. For cells infected with double-labelled virions (CA-eGFP 1:10), percentages of singly (IN-mCherry only; CA-eGFP-only) and double-labelled complexes (IN-mCherry + CA-eGFP) are plotted separately. Data are averages out of n=2 independent experiments. Statistical significance is indicated as * $p<0.05$ obtained with a Mann-Whitney test. Lack of statistical significance is not indicated. **E.** Summary table indicating the proportion of nuclear complexes out of total CA-eGFP and IN-mCherry complexes. Values are represented as mean ± SEM. Categories "IN-mCherry" and CA-eGFP" refer to the nuclear PICs containing only the respective label; double-labelled nuclear PICs are designated as "IN-mCherry+CA-eGFP" and "CA-eGFP+IN-mCherry", depending on whether the percentage of these complexes was calculated relative to the total number of all IN-mCherry- or all CA-eGFP labelled complexes, respectively.

Figure 13: HIV-1 entry model based on CA-eGFP labelling. Double-labelled virions, containing IN-mCherry and CA-eGFP enter the cells via fusion. Most CA-eGFP complexes dissociate from IN-mCherry complexes by 6 h post infection at the NE. CA-eGFP follows three pathways: majority (85%) of CA-eGFP is imported into the nucleus independently of IN-mCherry, a second portion (10%) is imported together with IN and a third portion remains associated at the nucleopore, possibly as an empty shell (5%). After import of complexes docked at the NE pores, IN-mCherry is associated with integration competent complexes, while the role of nuclear CA-eGFP complexes remains to be elucidated.

Accepted Manuscript Posted Online

Downloaded from http://jvi.asm.org/ on February 4, 2020 at 26989832

Tables

Table 1: Characteristics of IN-mCherry and CA-eGFP complexes in HeLa P4 cells at 6 h post infection.

A

	IN-mCherry								
	Cytoplasm			Nuclear envelope			Nucleus		
Virus	Intensity (a.u.)	Complexes/ cell	N	Intensity (a.u.)	Complexes/ cell	N	Intensity (a.u.)	Complexes/ cell	N
WT-mCh	0.741 ± 0.821	28.00 ± 10.75 (68%)	1121	0.546 ± 0.547	10.00 ± 5.50 (25%)	421	0.463 ± 0.191	2.00 ± 2.37 (6%)	99
CA-eGFP 1:2	0.796 ± 0.819	25.50 ± 10.06 (74%)	1194	0.520 ± 0.492	7.00 ± 4.74 (23%)	323	0.374 ± 0.164	0.50 ± 1.57 (3%)	50
CA-eGFP 1:10	0.994 ± 1.184	35.00 ± 12.48 (70%)	1049	0.692 ± 0.694	11.50 ± 4.98 (23%)	340	0.513 ± 0.252	2.50 ± 3.12 (7%)	99
	CA-eGFP								
	Cytoplasm			Nuclear envelope			Nucleus		
Virus	Intensity (a.u.)	Complexes/ cell	N	Intensity (a.u.)	Complexes/ cell	N	Intensity (a.u.)	Complexes/ cell	N
CA-eGFP 1:2	0.314 ± 0.271	15.50 ± 7.94 (41%)	612	0.275 ± 0.177	16.00 ± 10.56 (41%)	252	0.279 ± 0.178	6.00 ±5.35 (18%)	264
CA-eGFP 1:10	0.348 ± 0.272	15.00 ± 7.46 (38%)	469	0.260 ± 0.197	19.00 ± 7.44 (40%)	492	0.282 ± 0.186	9.50 ± 6.63 (22%)	302

B

	IN-mCherry + CA-eGFP					
	Cytoplasm		Nuclear envelope		Nucleus	
Virus	Complexes/cell	N	Complexes/cell	N	Complexes/cell	N
CA-eGFP 1:2	6.00 ± 4.71 (78%)	250	1.00 ± 1.18 (12%)	52	0.00 ± 0.86 (10%)	12
CA-eGFP 1:10	6.50 ± 4.59 (70%)	198	2.00 ± 2.05 (21%)	58	0.00 ± 0.50 (9%)	6

C

	Nuclear complexes/cell		
Virus	IN-mCherry only	CA-eGFP only	IN-mCherry + CA-eGFP
CA-eGFP 1:2	0.50 ± 1.57	7.00 ± 4.93	0.00 ± 0.86
CA-eGFP 1:10	6.00 ± 3.09	9.00 ± 6.57	0.00 ± 0.50

The table refers to Figure 7. HeLa P4 cells were infected with single- or double-labelled recombinant virions and fixed 6 h post infection. Viral complexes were identified and fitted to a 2D Gaussian by in-house Matlab routines. Based on nuclear lamina staining, the complexes were assigned as localizing in the cytoplasm, at the nuclear envelope or in the nucleus. Shown in tables are fluorescence intensities of identified complexes (in arbitrary units, a.u.) and numbers of complexes per cell (complexes/cell). All values are plotted as the median ± standard deviation. For both IN-mCherry and

Journal of Virology JVI Journal of Virology

Accepted Manuscript Posted Online

CA-eGFP complexes, the percentage of total complexes localizing in a specific intracellular compartment (cytoplasm, nuclear envelope, nucleus) is shown as percentage in brackets. N- total number of viral complexes identified in a subcellular compartment (cytoplasm, nuclear envelope, nucleus). Data are derived from one representative out of n=2 experiments. **A.** Numbers and fluorescence intensities of all identified IN-mCherry (upper panel) and CA-eGFP (lower panel) complexes in infected HeLa P4 cells. **B.** Numbers of complexes containing both IN-mCherry and CA-eGFP in infected HeLa P4 cells. In brackets, percentage of double-labelled complexes per compartment (cytoplasm, nuclear envelope, nucleus) is shown as the proportion of total double-labelled complexes. **C.** Overview of numbers of nuclear complexes, containing either one (IN-mCherry only, CA-eGFP only) or both (IN-mCherry + CA-eGFP) fluorescent labels.

Table 2: Numbers of fluorescent complexes in HeLa P4 cells transduced with virus-like particles (VLP) or enveloped viruses

		IN-mCherry complexes/cell				CA-eGFP complexes/cell			
Time	**Virus/VLP**	**Cytoplasm**	**Nuclear envelope**	**Nucleus**	**N**	**Cytoplasm**	**Nuclear envelope**	**Nucleus**	**N**
1.5 h	**WT-mCh VLP**	2.00 ± 3.07	0.00 ± 0.59	0.00 ± 0.00	85				
	CA-eGFP VLP	3.00 ± 3.88	0.00 ± 0.44	0.00 ± 0.00	83	1.00 ± 1.38	0.00 ± 0.26	0.00 ± 0.26	40
	WT-mCh	7.00 ± 8.40	1.00 ± 1.20	0.00 ± 0.00	242				
	CA-eGFP	8.50 ± 4.90	1.00 ± 1.92	0.00 ± 0.00	175	2.00 ± 1.62	1.00 ± 0.60	0.00 ± 0.36	54
6 h	**WT-mCh VLP**	2.00 ± 1.50	0.00 ± 0.31	0.00 ± 0.00	41				
	CA-eGFP VLP	2.00 ± 2.00	0.00 ± 0.47	0.00 ± 0.00	67	1.00 ± 1.66	0.00 ± 0.66	0.00 ± 0.31	52

Downloaded from http://jvi.asm.org/ on February 4, 2020 at 26989832

Journal of Virology JVI Journal of Virology

Accepted Manuscript Posted Online

	WT-mCh	9.50 ± 5.02	2.00 ± 1.55	0.00 ± 0.69	230				
	CA-eGFP	4.00 ± 3.66	0.00 ± 0.99	0.00 ± 0.16	222	2.00 ± 1.15	0.00 ± 1.25	0.00 ± 0.79	84

1304 Recombinant virus particles or virus-like particles (VLPs) were produced by transient transfection of
1305 the HIV-1 vector system, as described in Methods, with or without the VSV-G encoding construct,
1306 respectively. Viruses and VLPs were purified and concentrated and particle release was assessed by
1307 p24 ELISA. Identical particle amounts (determined by p24 ELISA) were used to synchronously
1308 transduce HeLa P4 cells, which were fixed and immunostained with nuclear lamin antibodies at 1.5 h
1309 (upper panel) or 6 h (lower panel) post transduction. Viruses containing IN-mCherry (WT-mCh) or IN-
1310 mCherry and CA-eGFP (CA-eGFP 1:10) are annotated by VSV-G label, whereas the corresponding
1311 VLPs are indicated by ΔVSV-G. The complex numbers are shown per intracellular compartment in
1312 which they were found (cytosol, nuclear envelope, nucleus), based on lamin staining. The values
1313 shown represent median ± standard deviation. The total number of complexes from which data are
1314 derived is plotted in the last column (N).

1315

1316

1317

1318 **Table 3: Characteristics of IN-mCherry and CA-eGFP complexes in HeLa P4 cells 1.5 h post infection**
1319 **(p.i.).**

A

		IN-mCherry complexes/cell (1.5 h)			IN-mCherry intensity (a.u.) (1.5 h)			
	Virus	**Cytoplasm**	**Nuclear envelope**	**Nucleus**	**Cytoplasm**	**Nuclear envelope**	**Nucleus**	**N**
DMSO	**WT-mCh**	4.00 ± 3.19	0.00 ± 0.63	n.v.	1.431 ± 2.650	1.080 ± 0.604	n.v.	283
	CA-eGFP	10.00 ± 6.49	2.00 ± 1.77	0.00 ± 0.16	1.708 ± 1.884	1.839 ± 2.240	0.984 ± 0.277	918
2 µM PF74	**WT-mCh**	4.50 ± 3.66	0.00 ± 0.84	n.v.	1.679 ± 2.697	1.156 ± 1.267	n.v.	381
	CA-eGFP	12.00 ± 6.02	1.00 ± 1.95	n.v.	1.890 ± 2.534	2.246 ± 2.141	n.v.	1009
10 µM PF74	**WT-mCh**	5.00 ± 4.03	0.00 ± 0.78	n.v.	1.927 ± 1.618	1.654 ± 1.171	n.v.	346
	CA-eGFP	11.00 ± 5.69	1.00 ± 1.94	n.v.	2.041 ± 2.324	2.077 ± 2.437	n.v.	997

1320

Journal of Virology
JVI
Journal of Virology
Downloaded from http://jvi.asm.org/ on February 4, 2020 at 26989832

Accepted Manuscript Posted Online

Journal of Virology

JVI

Journal of Virology

Downloaded from http://jvi.asm.org/ on February 4, 2020 at 26989832

B		CA-eGFP complexes/cell (1.5 h)			CA-eGFP intensity (a.u.) (1.5 h)			
	Virus	Cytoplasm	Nuclear envelope	Nucleus	Cytoplasm	Nuclear envelope	Nucleus	N
DMSO	CA-eGFP	2.00 ± 3.29	1.00 ± 1.85	0.00 ± 1.14	0.839 ± 0.648	0.682 ± 0.453	0.786 ± 0.292	380
2 µM PF74		3.00 ± 3.17	1.00 ± 1.19	0.00 ± 0.15	0.775 ± 0.640	0.620 ± 0.313	0.296 ± 0.000	209
10 µM PF74		1.50 ± 1.39	0.00 ± 1.06	0.00 ± 0.29	0.774 ± 0.722	0.512 ± 0.644	0.561 ± 0.343	152

HeLaP4 cells were transduced with single- (WT-mCh) or double-labelled (CA-eGFP) virus particles, in the presence of either DMSO or PF74 (2 µM or 10 µM) and fixed 1.5 h post infection. Fluorescent virus complexes were localized and fitted with a 2D Gaussian curve. Integrated intensity was calculated in each z-section. The experiment was performed twice, and the mean of all data are shown. The data were collected from 50-60 cells corresponding to approximately 500 IN-mCherry (**A**) and 300 CA-eGFP (**B**) complexes detected in total. The complex numbers are shown per intracellular compartment in which they were found (cytosol, nuclear envelope, nucleus), based on lamin staining. The values shown represent median ± standard deviation. The total number of complexes from which data are derived is plotted in the last column (N).

Table 4: **Characteristics of IN-mCherry and CA-eGFP complexes in HeLa P4 cells 6 h post infection (p.i.).**

A		IN-mCherry complexes/cell (6 h)			IN-mCherry intensity (a.u.) (6 h)			
	Virus	Cytoplasm	Nuclear envelope	Nucleus	Cytoplasm	Nuclear envelope	Nucleus	N
DMSO	WT-mCh	14.00 ± 10.95	3.00 ± 3.81	0.00 ± 0.86	1.164 ± 1.147	0.956 ± 1.081	0.768 ± 0.495	1572
	CA-eGFP	20.00 ± 10.34	3.00 ± 2.38	0.00 ± 0.90	1.094 ± 1.380	0.936 ± 0.974	0.633 ± 0.248	1775
2 µM PF74	WT-mCh	12.50 ± 10.17	2.00 ± 3.38	0.00 ± 0.34	1.092 ± 1.003	1.046 ± 0.899	0.828 ± 0.579	1710
	CA-eGFP	12.00 ± 9.02	4.00 ± 2.48	0.00 ± 0.19	1.107 ± 1.280	1.060 ± 1.411	0.578 ± 0.000	1438
10 µM PF74	WT-mCh	11.00 ± 6.92	1.00 ± 1.30	0.00 ± 0.12	1.257 ± 1.473	1.231 ± 1.640	0.422 ± 0.000	983
	CA-eGFP	13.00 ± 7.33	1.00 ± 1.47	0.00 ± 0.13	1.224 ± 1.381	1.165 ± 1.296	0.499 ± 0.000	886

Accepted Manuscript Posted Online

B

		CA-eGFP complexes/cell (6 h)			CA-eGFP intensity (a.u.) (6 h)			
	Virus	**Cytoplasm**	**Nuclear envelope**	**Nucleus**	**Cytoplasm**	**Nuclear envelope**	**Nucleus**	**N**
DMSO	**CA-eGFP**	5.00 ± 3.25	2.00 ± 2.34	3.00 ± 3.63	0.370 ± 0.427	0.391 ± 0.304	0.333 ± 0.202	866
2 µM PF74		6.50 ± 8.32	2.00 ± 1.55	0.00 ± 0.61	0.494 ± 0.478	0.538 ± 0.447	0.575 ± 0.201	920
10 µM PF74		4.00 ± 2.74	1.00 ± 0.90	0.00 ± 0.18	0.376 ± 0.411	0.378 ± 0.491	0.120 ± 0.060	311

The table refers to Figure 9. HeLa P4 cells were transduced with single- (WT-mCh) or double-labelled (CA-eGFP) virus particles, in the presence of either DMSO or PF74 (2 µM or 10 µM) and fixed 6 h post infection. Fluorescent virus complexes were localized and fitted with a 2D Gaussian curve. Integrated intensity was calculated in each z-section. The experiment was performed twice, and the mean of all data are shown. The data were collected from 50-60 cells corresponding to approximately 1000 IN-mCherry (**A**) and 600 CA-eGFP (**B**) complexes detected in total. The complex numbers are shown per intracellular compartment in which they were found (cytosol, nuclear envelope, nucleus), based on lamin staining. The values shown represent median ± standard deviation. The total number of complexes from which data are derived is plotted in the last column (N).

Journal of Virology
JVI
Journal of Virology
Downloaded from http://jvi.asm.org/ on February 4, 2020 at 26989832

Accepted Manuscript Posted Online

Journal of Virology

JVI

Journal of Virology

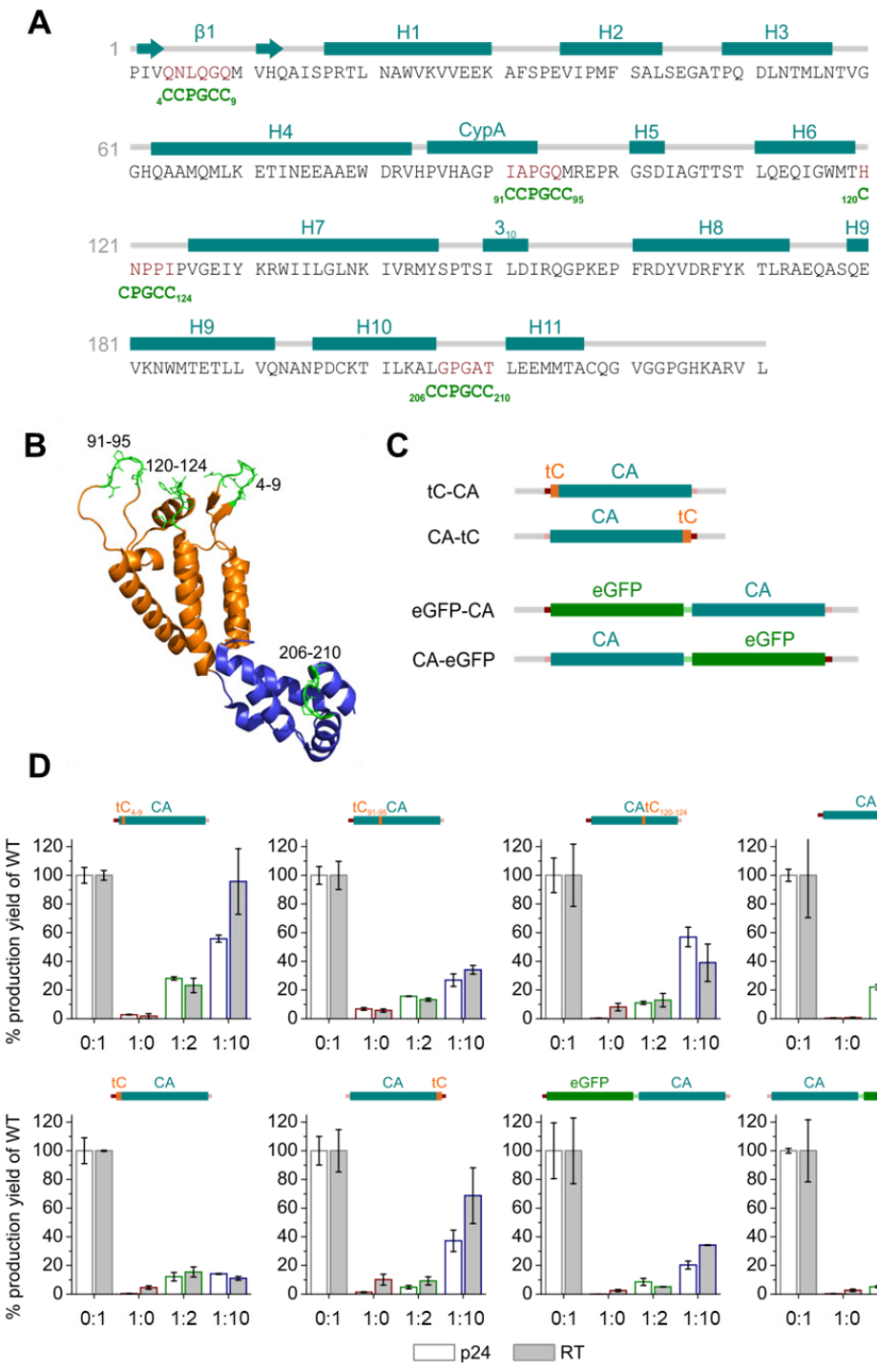

Downloaded from http://jvi.asm.org/ on February 4, 2020 at 26989832

Accepted Manuscript Posted Online

Journal of Virology

JVI

Journal of Virology

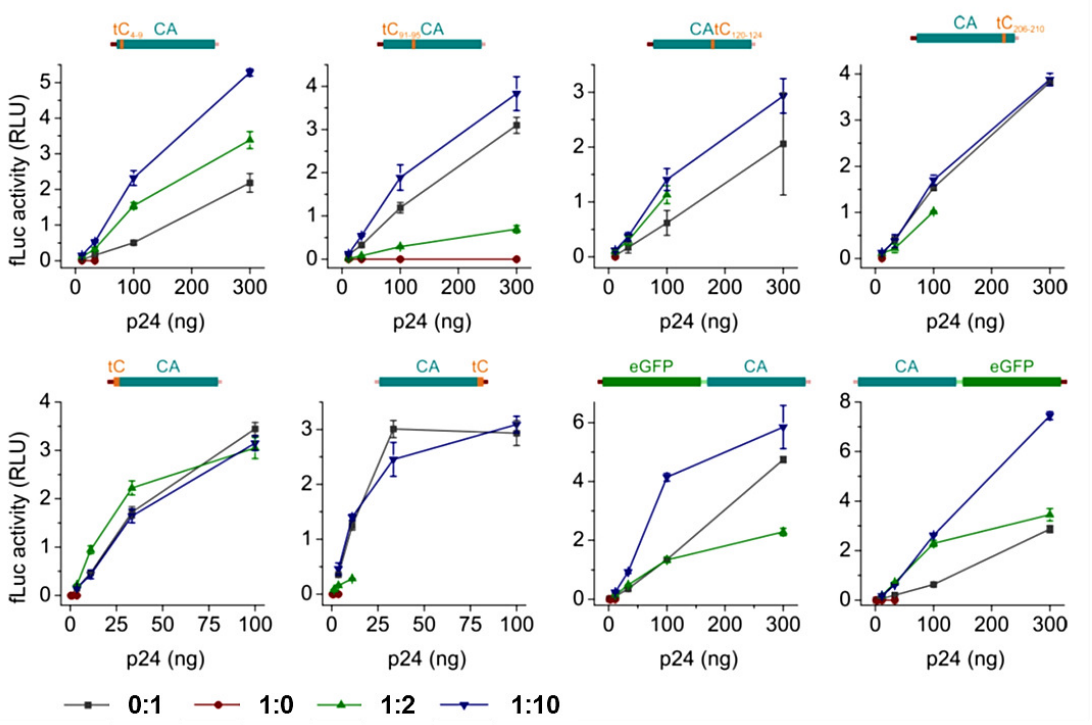

Downloaded from http://jvi.asm.org/ on February 4, 2020 at 26989832

Accepted Manuscript Posted Online

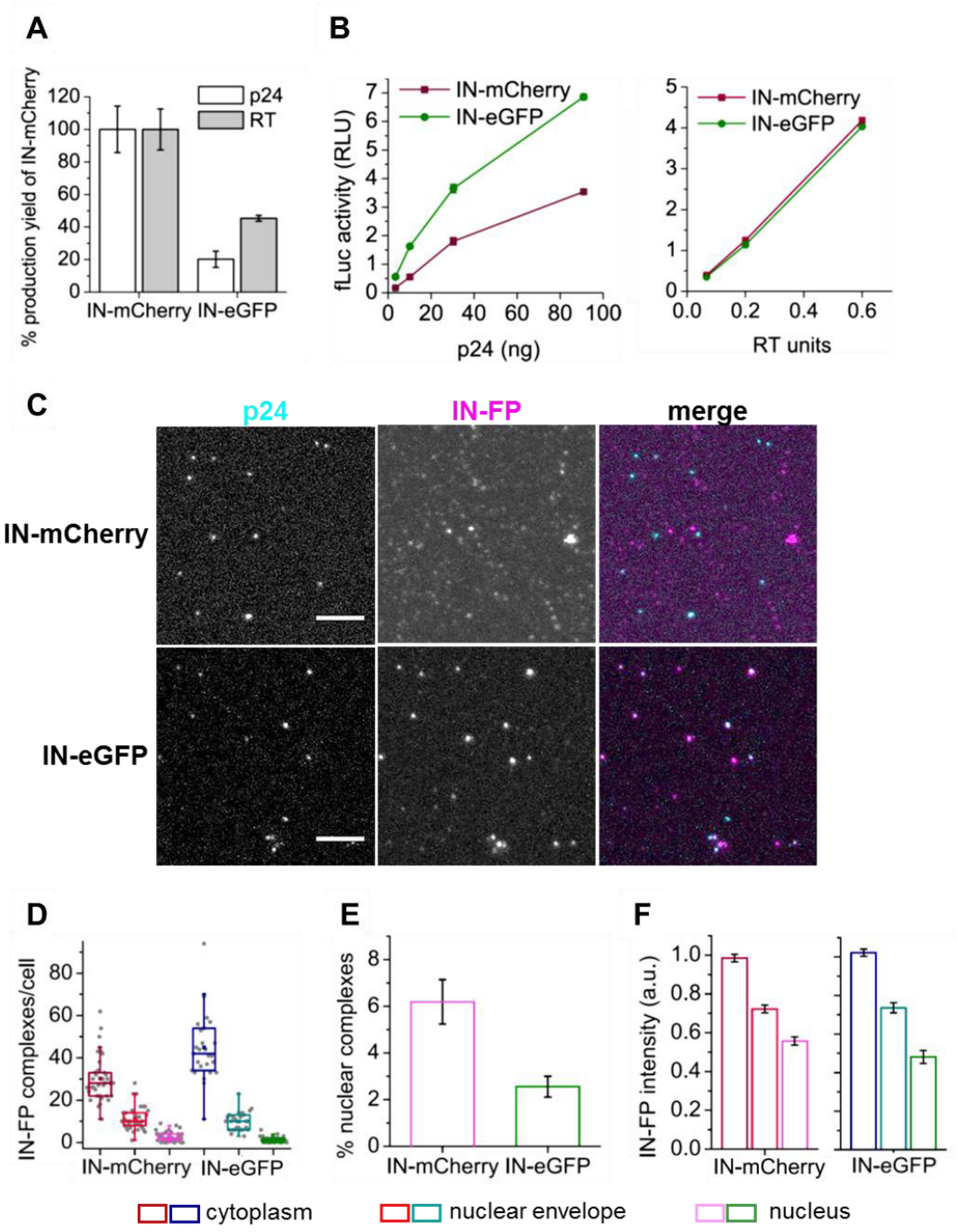

Downloaded from http://jvi.asm.org/ on February 4, 2020 at 26989832

JVI Journal of Virology

Journal of Virology

Accepted Manuscript Posted Online

Journal of Virology

JVI

Journal of Virology

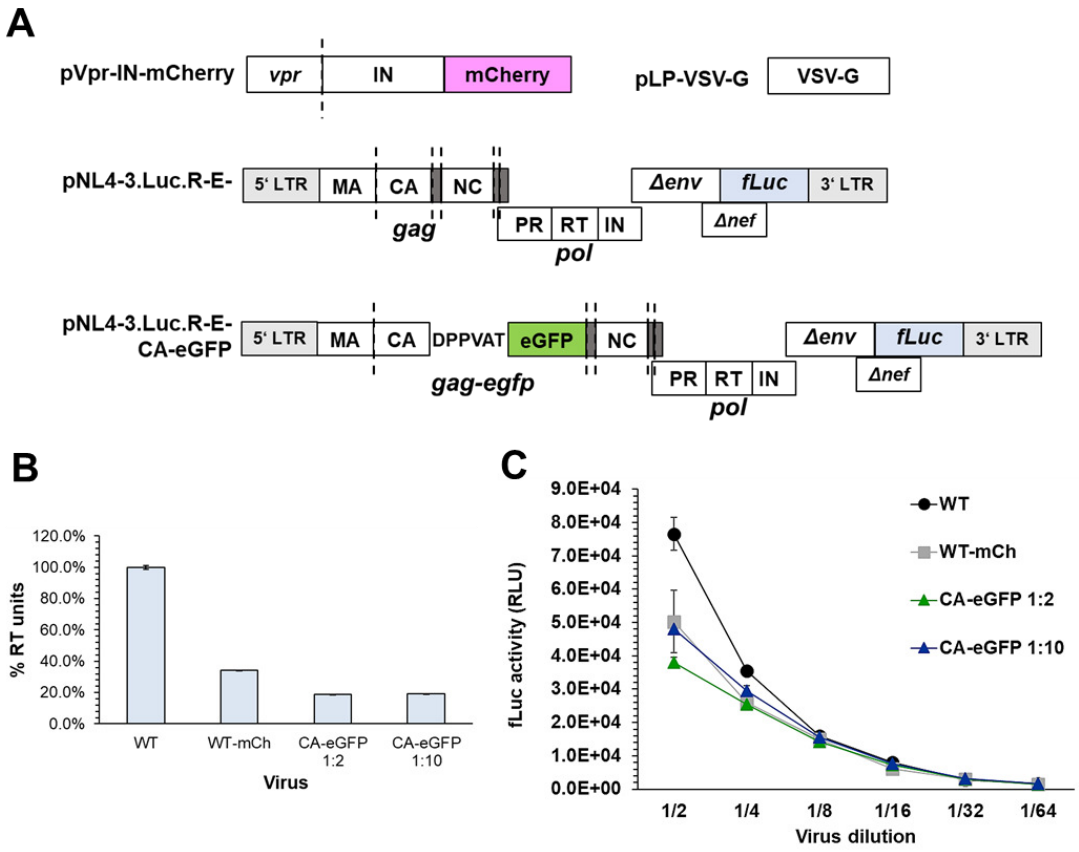

Downloaded from http://jvi.asm.org/ on February 4, 2020 at 26989832

Accepted Manuscript Posted Online

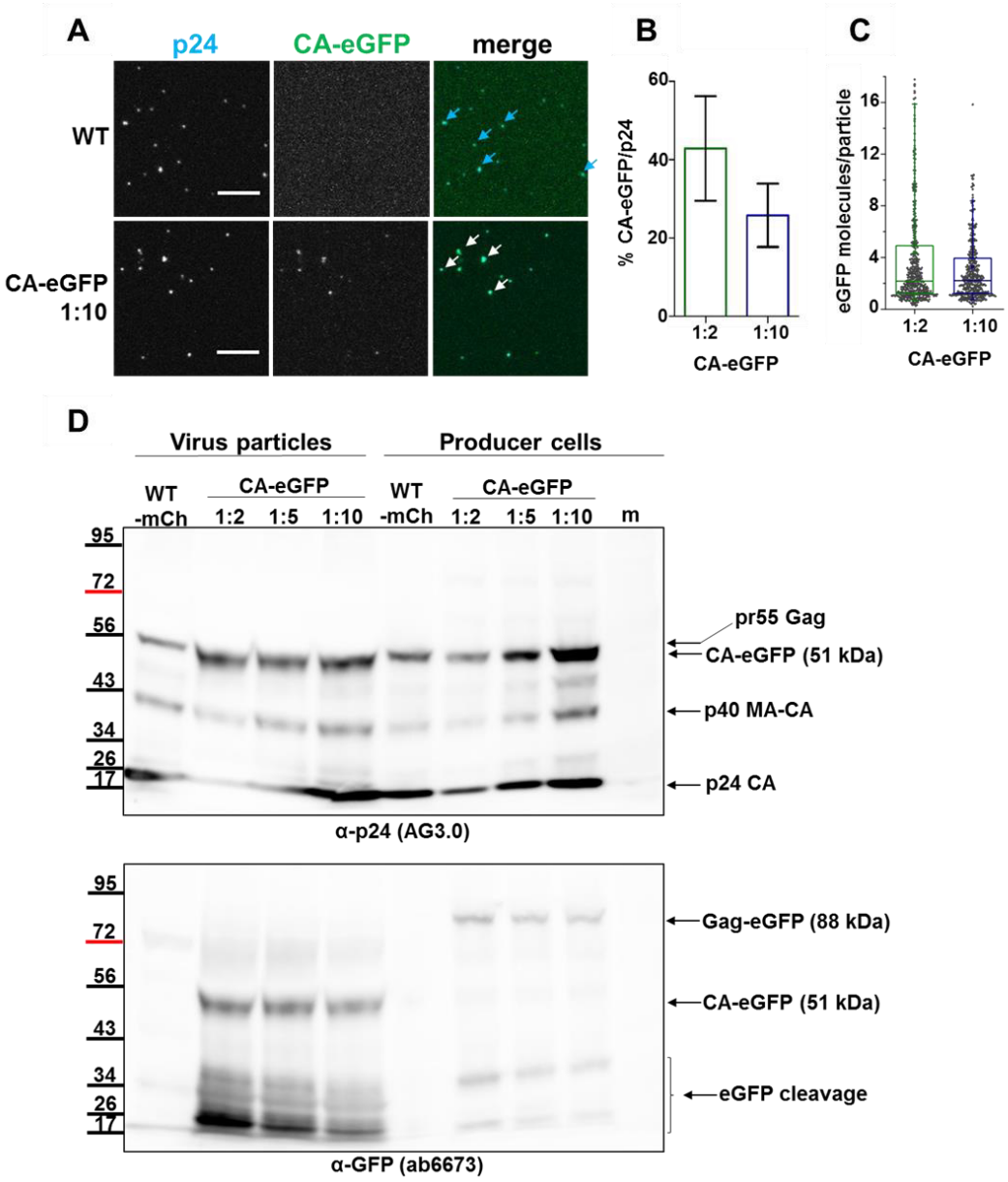

Downloaded from http://jvi.asm.org/ on February 4, 2020 at 26989832

Journal of Virology
JVI
Journal of Virology

Accepted Manuscript Posted Online

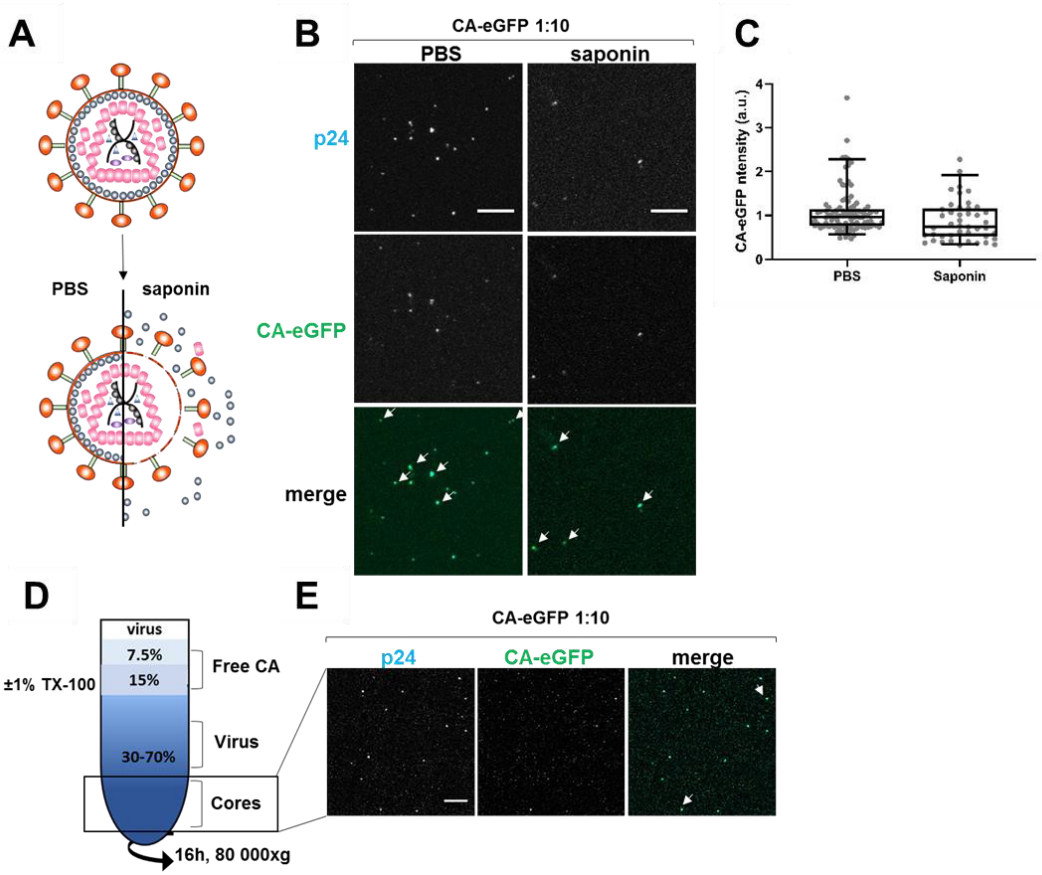

Downloaded from http://jvi.asm.org/ on February 4, 2020 at 26989832

Journal of Virology
JVI
Journal of Virology

Accepted Manuscript Posted Online

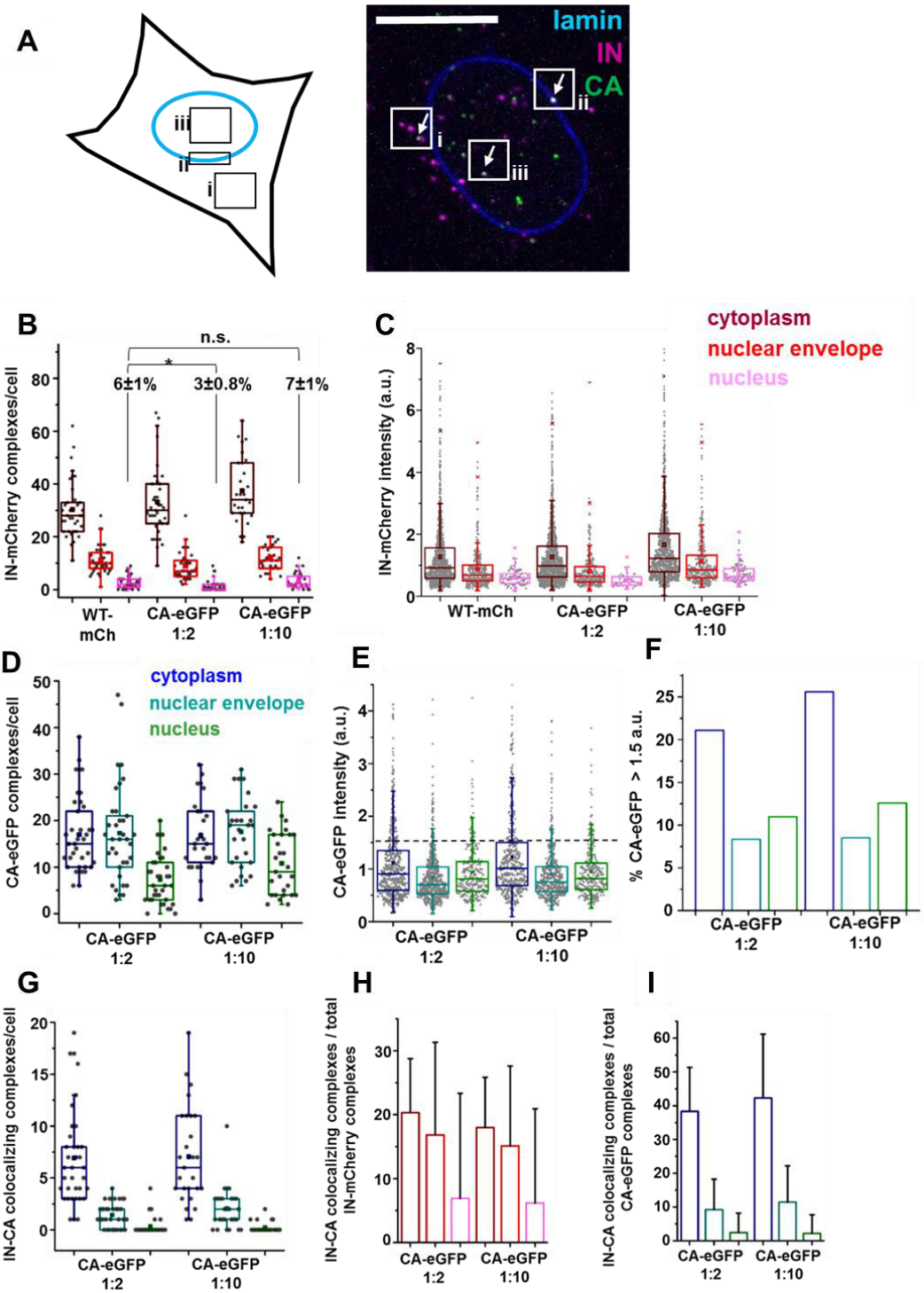

Downloaded from http://jvi.asm.org/ on February 4, 2020 at 26989832

JVI Journal of Virology

Journal of Virology

Accepted Manuscript Posted Online

Journal of Virology

JVI

Journal of Virology

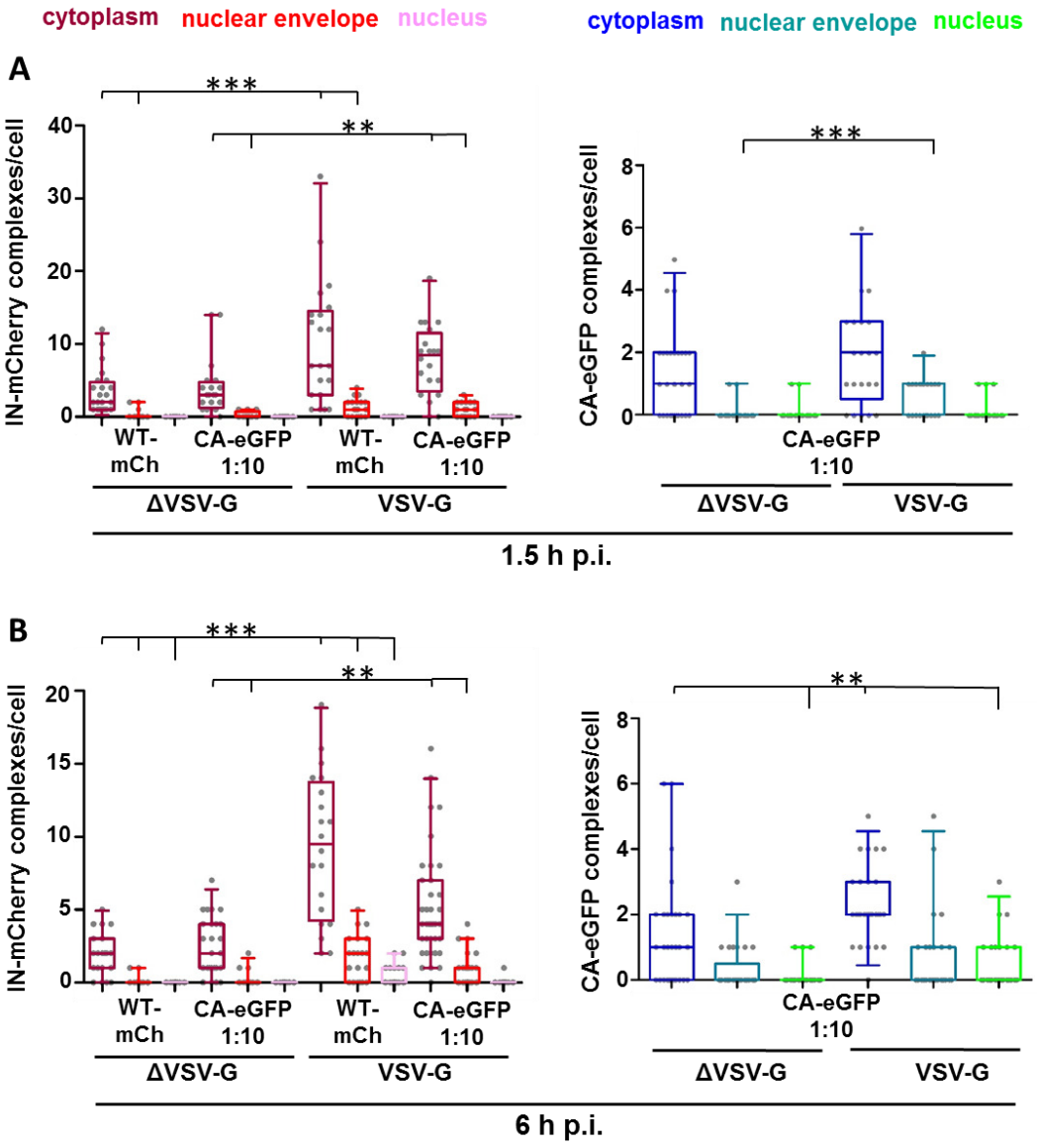

Downloaded from http://jvi.asm.org/ on February 4, 2020 at 26989832

Accepted Manuscript Posted Online

Journal of Virology

JVI

Journal of Virology

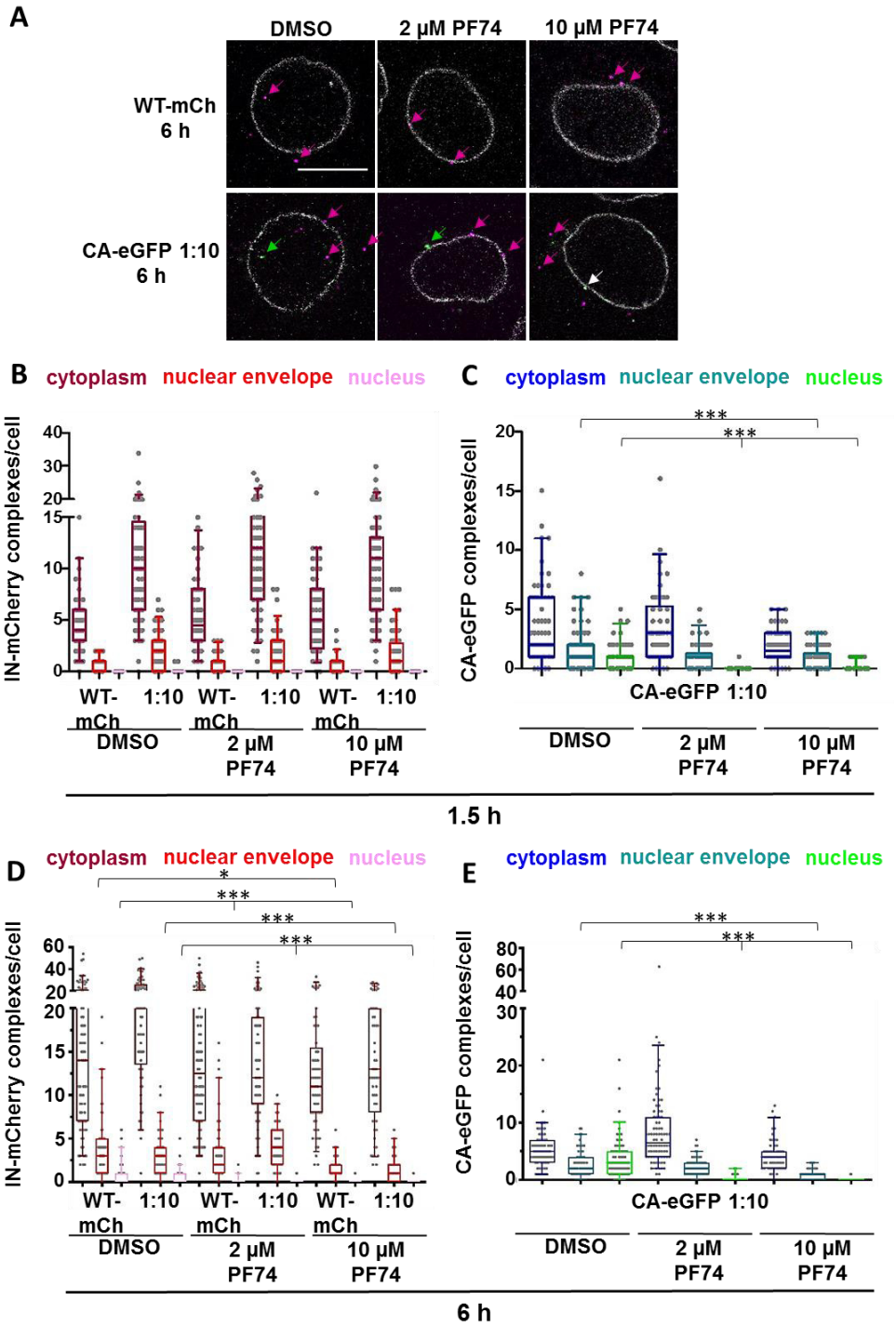

Downloaded from http://jvi.asm.org/ on February 4, 2020 at 26989832

Accepted Manuscript Posted Online

Journal of Virology

JVI

Journal of Virology

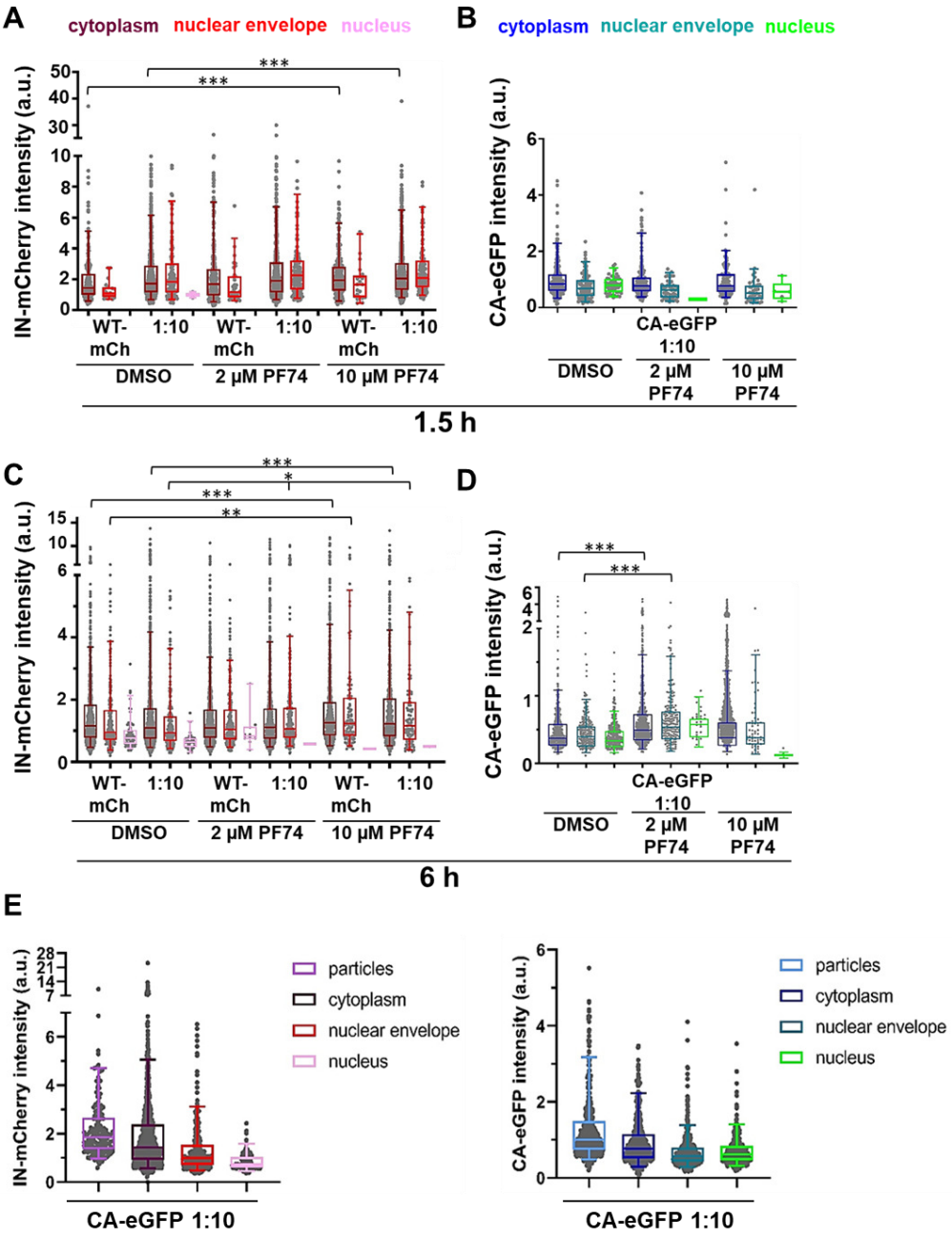

F

IN-mCherry				CA-eGFP			
particles	cytoplasm	nuclear envelope	nucleus	particles	cytoplasm	nuclear envelope	nucleus
1.847 ± 1.292	1.435 ± 1.710	0.999 ± 1.002	0.741 ± 0.364	1.009 ± 0.833	0.770 ± 0.601	0.574 ± 0.435	0.623 ± 0.412

Downloaded from http://jvi.asm.org/ on February 4, 2020 at 26989832

Accepted Manuscript Posted Online

Journal of Virology

JVI

Journal of Virology

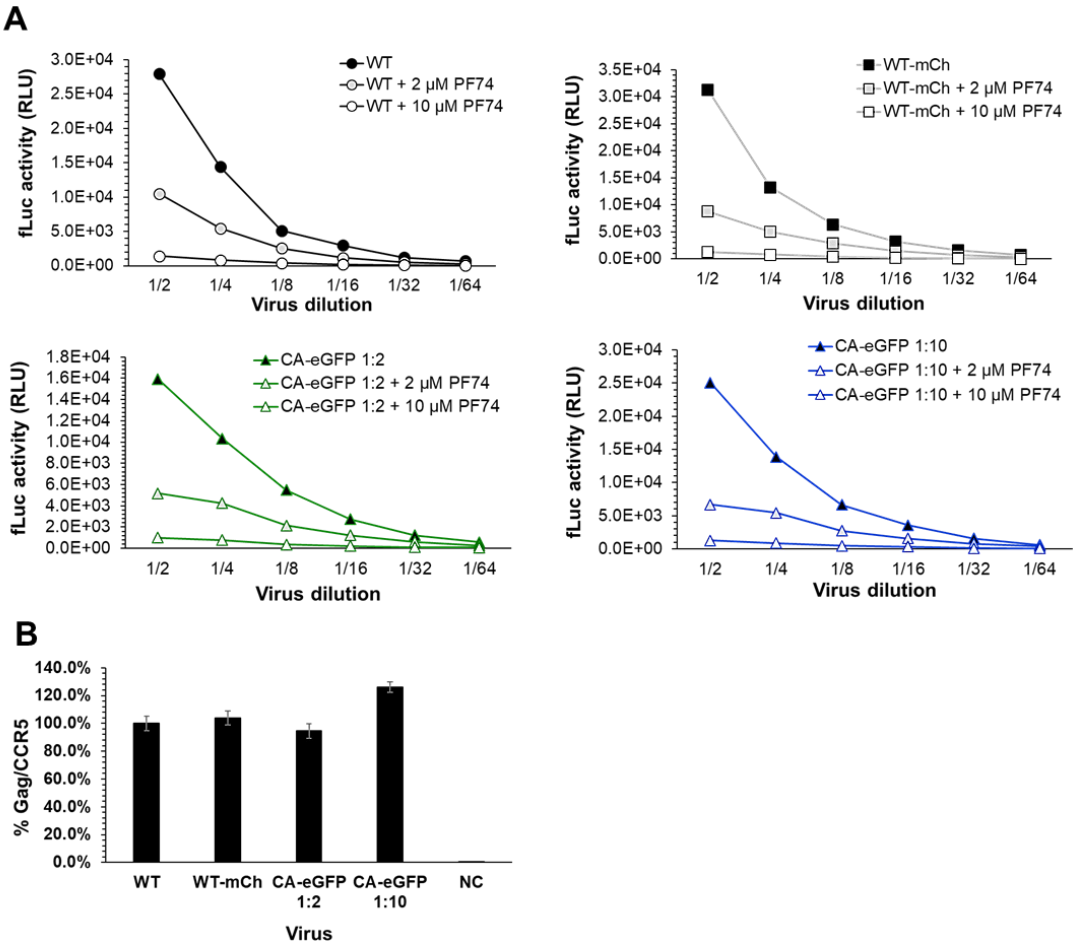

Downloaded from http://jvi.asm.org/ on February 4, 2020 at 26989832

Accepted Manuscript Posted Online

Journal of Virology

JVI

Journal of Virology

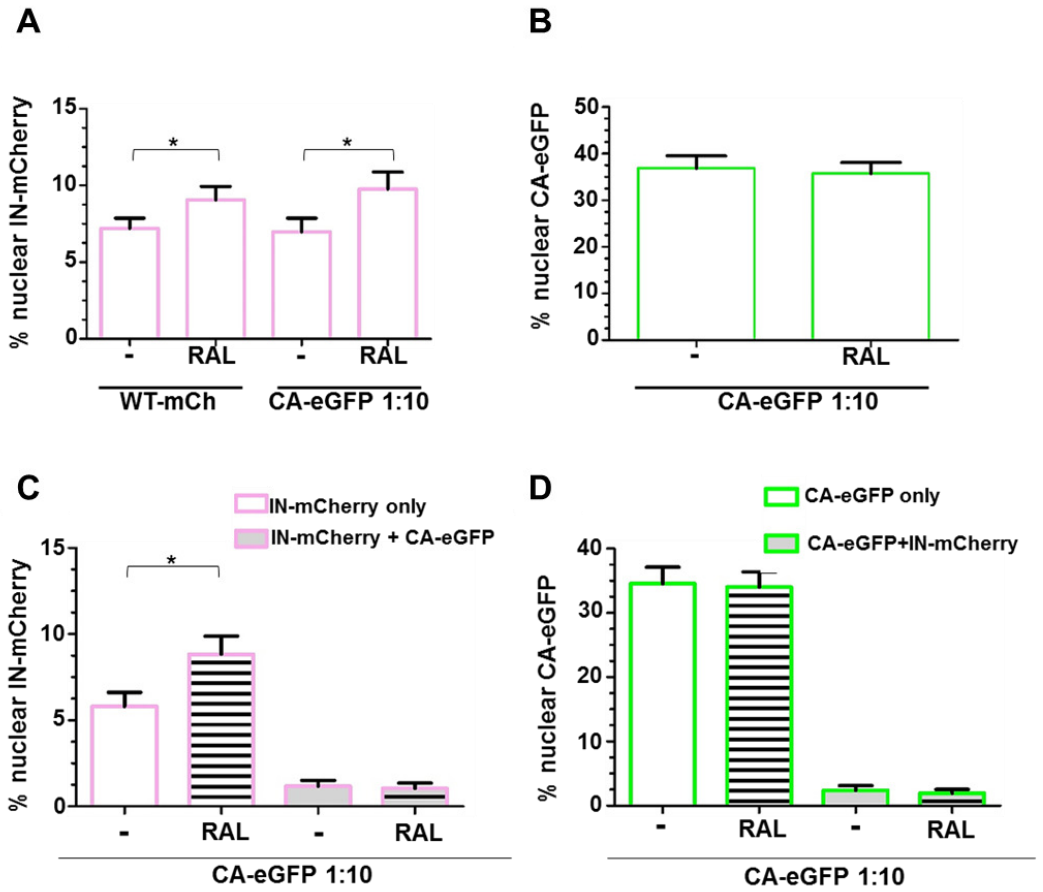

E

	% nuclear IN-mCherry complexes		% nuclear CA-eGFP complexes	
	IN-mCherry	IN-mCherry + CA-eGFP	CA-eGFP	CA-eGFP + IN-mCherry
DMSO	5.81 ± 0.81	1.17 ± 0.34	34.55 ± 2.56	2.37 ± 0.76
RAL	8.83 ± 1.06	1.04 ± 0.31	34.03 ± 2.35	1.97 ± 0.55

Downloaded from http://jvi.asm.org/ on February 4, 2020 at 26989832

Accepted Manuscript Posted Online

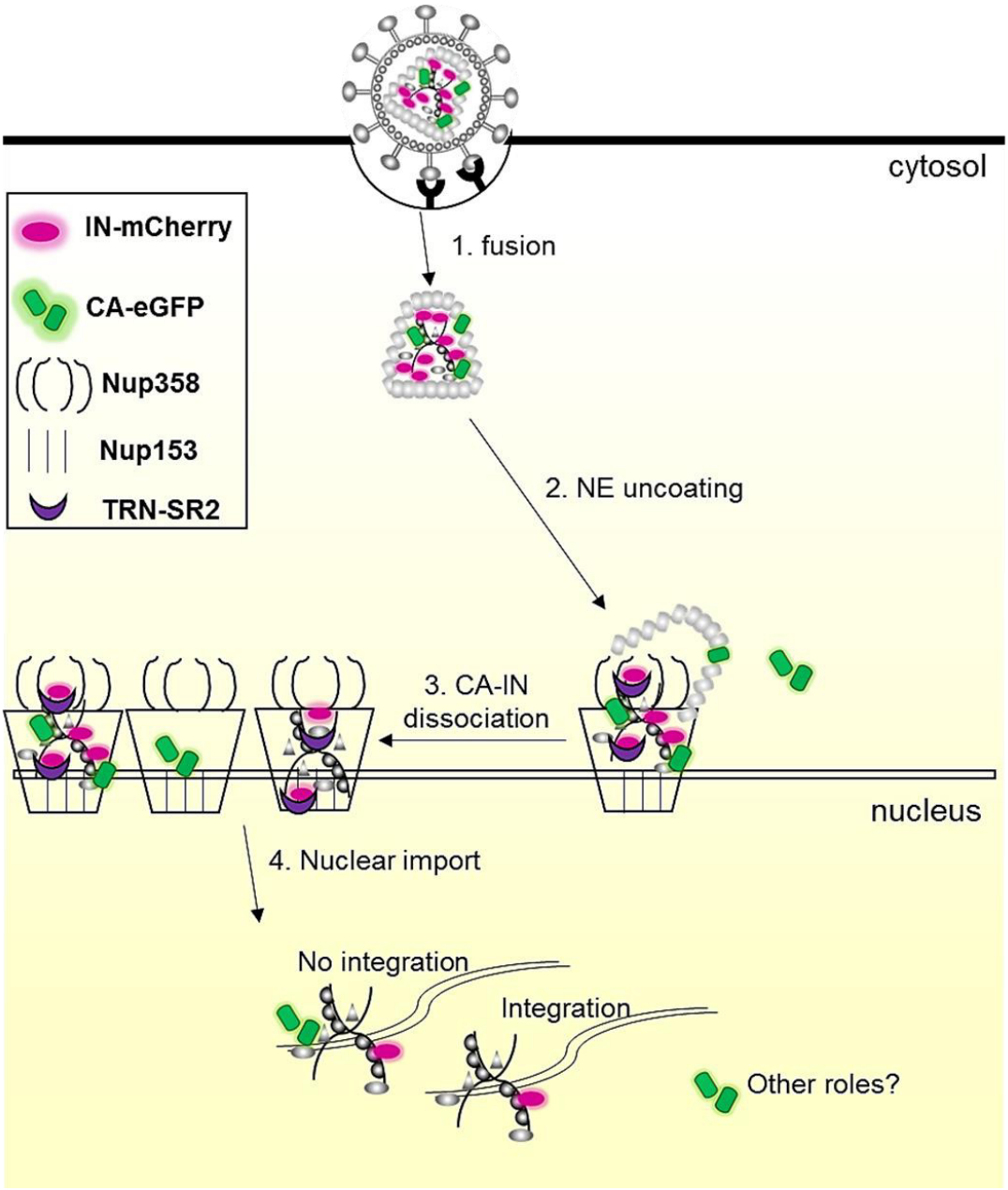

Downloaded from http://jvi.asm.org/ on February 4, 2020 at 26989832

Journal of Virology JVI Journal of Virology